Characterizing Volcanic and Impact Materials in Lunar Craters

Authored by Gwen Robbins

Submitted to the Department of Astronomy at Mount Holyoke College

with the purpose of honors consideration

Thesis Advisor:

Dr. Darby Dyar

United States Geological Survey (USGS) Advisor:

Dr. Lillian Ostrach

May 2022

Abstract

Impact craters on the Moon are typically infilled by either impact or volcanic melt, but outside of a few previously known characteristics, identification can be complicated. Morphological and compositional characteristics are the best options for definitive differentiation between volcanic and impact in impact craters. In this paper the history of lunar morphological research is reviewed and eight craters >60km in diameter are mapped to create a comprehensive list of features of note using the maps available through JMARS. Over the past 50 years, interest in lunar morphology has been primarily impacted by the technology available. Without high definition views of the lunar surface, studies on the Moon's craters focused on size and volume instead of internal components. As technology improved, the study of lunar craters expanded. This thesis shows that many features of note in impact melt-filled impact craters exist primarily on the crater floor. That floor has been obscured in volcanically-filled impact craters. Impact melt-filled impact craters also maintain the same albedo and composition as the surrounding terrain, while volcanically-filled impact craters are of a darker albedo and mafic composition. The existence of terraced rims is affected by age rather than interior fill composition, unless the interior melt has obscured any terraces. Crater rims slump with age and therefore cannot indicate alone the type of melt inside the crater.

Acknowledgments

The land on which most of this research was conducted is the traditional unceded territory of the Hohokam, Hopi, Pueblos, and Apache Nations. Iacknowledge the painful history of genocide, forced relocation, and occupation of their territory. Northern Arizona University sits at the base of the San Francisco Peaks, which are sacred to 13 tribes. The land was never ceded by these nations and is occupied detrimentally by the Snowbowl ski resort. Astronomy and illegal land occupation are intertwined and as astronomers it is our responsibility to concede to the requests of the indigenous populations whose land we are on. I firmly believe that tribal lands should be returned to the populations from which it was stolen, particularly in Hawaii and Arizona, which are places of high astronomical impact.

I’d like to thank Dr. Darby Dyar and Dr. Lillian Ostrach for all their support on this thesis. I could never have done this without you. Thank you so much for everything. Special thanks to Dr. Jason Young and Dr. Spencer Smith for being on my committee on such a short notice. You have all supported me throughout my research and overall college experience and it means so much to me. Thank you. I’d also like to thank Dr. Roslyn Eisenberg, my grandmother, who fostered and supported my career. I wish you could have read this. And a final thank you to my roommates, Riannon, Jasmine, and Josie, who supported me all year.

Table of Contents

List of Figures and Tables

1: Introduction and Objective

The Moon (Fig. 1) has three major geologic processes that alter its surface: tectonics, volcanism, and impact events. The latter two of these processes can be directly observed on the surface. Impact craters form when an impactor, typically a small piece of debris leftover from solar system formation, collides with the surface at high speeds. The crust bends and moves away from the impact site like a liquid before settling or flowing back down into the new bowl. Larger impactors reach such high speeds that the energy released at impact actually melts the surface, resulting in what is called impact melt. The liquified crust cools over time, solidifying into place. However, this is not the only melt found on the lunar surface. There are currently no confirmed sources for volcanism. Eventually, volcanic melt rises from beneath the surface into low-lying impact craters and covers up the impact melt before solidifying into a smooth, dark flows called volcanic melt or mare, terms used interchangeably here. Galileo first coined the term ‘maria’, meaning ‘seas’, to refer to the dark patches on the nearside of the Moon (Wood, 2018) when he looked at the Moon telescopically. What was believed to be a smooth surface were craters, canyons, and mountains. Telescopic mapping of the Moon’s nearside continued into the following centuries with a focus on searching for changes on the Moon (that were not there).

Figure 1: The nearside of Earth's Moon, as seen based on data from cameras aboard NASA's robotic Lunar Reconnaissance Orbiter spacecraft.

Image Credit: NASA/Goddard Space Flight Center/Arizona State University

Johann Hieronymus Schröter first noticed a correlation between crater depth and diameter in his 1791 piece “Selenotopographische Fragmente” (Koeberl, 2001), though at the time he claimed craters were created by volcanic activity. In fact, scientists believed lunar craters formed volcanically well into the 20th century (Wood, 2018, Koeberl, 2001, Melosh, 1996). Because there was no known mechanism for consistently producing circular impact craters, impacts could not be the primary cause of crater formation (Wood, 2018). However, a lack of any present volcanic activity, or even volcanic origin, soured these claims. Attitudes towards impact theory shifted in the 20th century as studies into impact theory emerged (Racki et al., 2014), claiming that impactors had higher velocities than previously believed and therefore consistently created round craters regardless of impact velocity (Koeberl, 2001). By the 1960s, impact theory dominated the academic landscape with the groundwork for basic crater understandings laid out by the United States Geological Survey (Wood, 2018). However uncertainty persisted up until the Apollo Moon landings in 1969, which confirmed craters to be impact in origin (Koeberl, 2001, Wood, 2018). The truth of impact theory does not negate volcanic activity on the Moon. Lunar maria comes from volcanic sources, however the exact source of mare deposits remains a topic of debate.

As our understanding of the Moon has progressed, several individual topics pertaining to surface characteristics emerged over the years. The following paragraphs introduce these topics, as well as the findings pertaining to impact melt material and mare material. Because lunar craters have been heavily studied and imaged, there are a considerable amount of data available to identify key traits in each fill type.

Identification of impact melt on the Moon and other surfaces is typically based on three primary characteristics: interior pond morphology (smooth texture, distinct crater-fill boundaries, few to no superimposed craters), a lack of embayed craters (craters that have been filled in leaving only the rim visible), and the presence of exterior deposits (i.e. exterior ponds and veneers) (Ostrach et al., 2012). However, identification of these features requires a young crater that is still intact, so that degradation has not significantly affected its surface. Volcanic fill is primarily identified as having a lower albedo than the surrounding terrain. The filled-in crater may also have secondary craters completely filled except for the remaining rim, called embayed craters. These features all are distinctly visible by eye when looking at a broad view of the Moon, therefore the type of fill can be easily identified using key characteristics. But these features are not concrete evidence towards one type of fill. In fact, some craters that were previously believed to be created by one form of melt emplacement have later been determined to be otherwise (Ashley, 2012). Classification requires a more robust set of criteria that can fit craters of all ages and shapes, and developing a classification is a goal of this thesis.

In the first part of this thesis, craters are characterized and classified by examining the history of lunar morphology research in depth. The past five decades have provided a comprehensive list of features to expect or look for within craters, as well as inform the biases and current state of research into lunar craters. The numerous characteristics previously attributed to lunar craters are analyzed, pointing to specific characteristics that seem ubiquitous or of note in my study.

In the second part of this thesis, in-depth analysis of eight craters is used to create a more comprehensive list of characteristics for observed features hosted within impact melt-filled craters that contain volcanic infill and impact interior fill. The goal is to develop more definitive criteria for identifying these important features. The Lunar

Reconnaissance Orbiter Camera (LROC) took images used to provide valuable insights into morphological characteristics beyond these previously listed. High-definition images from the Narrow Angle Cameras (NAC) and Wide Angle Camera (WAC) cameras aboard LROC were used to photograph eight craters with a diameter >30km with both types of fill and varying in age and location. Using these images, morphological traits common to each type of fill were identified. Comparisons among several craters are crucial for a study of this kind, as common traits may be attributed to several factors beyond fill type.

This project aspires to create a useful tool for the community to apply when looking at craters both on the Moon and beyond. As our closest neighbor, the Moon has the most resources for studying impact craters in depth. While not all of the processes prevalent on the Moon may be directly applied elsewhere, certain characteristics may serve as a benchmark for examining impact craters on other bodies. Should an impact crater on another planetary body feature some of the same traits as seen on the Moon, it may be a fair assumption that their formation processes are similar.

2: Background

This chapter covers the past five decades of lunar morphological research in depth. It is divided by the specific qualities of lunar morphology, as well as a brief description of the history of this area of study. This summary of the history of lunar morphology research applies and contextualizes the current understanding of craters on the Moon.

2.1: Size and volume of craters and mare

Research into lunar morphology in the late 20th century focused on size and depth of impact craters (Head and Wilson, 1991, Cintala and Grieve, 1998, Melosh and Ivanov, 1999, Smith, 1976). The diameter and depth of an impact crater are directly related (Head, 1991) and are determined by the size of the original impactor. This relationship is given by a ratio between depth (d) and diameter (D) and written as d/D. Until lunar missions in the 1990s, a majority of academic papers focused on classifying craters at certain sizes and depths, understanding cratering mechanisms, and determining the thickness of the lunar crust (Smith, 1976, Head, 1976, Head and Wilson, 1991). Crust on the nearside can be separated into lunar highlands and maria, while the far side is majorly highlands (Jaumann et al., 2012) with small pockets of mare only in craters. In 1990 and 1992, Galileo flew by the Moon en route to Jupiter and gained the first multispectral images of the lunar surface in decades (Hiesinger and Head, 2006). The laser altimeter onboard Clementine provided the first global map of lunar topography (Hiesinger and Head, 2006), and subsequent missions improved topographic resolution and revealed previously unmapped impact basins and undistinguishable features (Hiesinger and Head, 2006, Neumann et al., 2015).

Visible maria make up approximately 17% of total surface area, yet comprises only 1% of crust volume (Head and Wilson, 1991). Nearside maria have an average thickness of less than 400m, with small pockets reaching 1-2km deep (Dehon and Waskom, 1979). Mare flows in several thin increments over millions of years, with each flow approximately 10-15m thick (Jaumann et al., 2012, Hiesinger and Head, 2006), though initially volume estimates for deposits operated under the assumption of large-scale flows (Robinson et al., 2012). Impact-filled crater floors are the largest source of impact melt inside craters (Dhingra et al., 2017). The volume of crater fill generated during impact events and the morphology of the resulting melt flows are directly related to the preexisting topography and diameter of the crater created (Lev et al., 2021). Intense pressure during the impact event causes rock to act like a fluid (Holsapple, 1989) and pushes flow towards areas of lower pressure (Melosh, 1989), dictating the final appearance of each crater.

Initial observations of the Moon concluded that craters <10km in diameter mostly contained veneers and small ponds, while craters 20-50km in diameter were more likely to have melt flow (Carter et al., 2012). The smaller craters were simply labeled as “crater material” (Kruger et al., 2016). Though these features are now known to be more universal, these findings were an early criterion for distinguishing among types of craters. Two types of craters, simple and complex, each have distinct features and specific size boundaries; craters with a diameter less than 15km are simple (Williams and Zuber, 1998) and may differ in formation mechanism (Lev et al., 2021). Simple craters are determinable by a bowl-like interior, unterraced rims (in this paper a terraced rim refers to a smooth level surface at higher elevation than the crater floor), and visible ejecta (Jaumann et al., 2012, Melosh, 1989). Previous datasets show impact melt exterior flow and central peaks unlikely in craters <10km (Smith, 1976). However, increased resolution from Lunar Reconnaissance Orbiter (LRO) (Robinson et al., 2010) supports flow outside craters >600m in diameter (Neish et al., 2014). Transition to complex crater types occurs when the crater rim wall slumps into terraces (Melosh and Ivanov, 1999, Williams and Zuber, 1998) at around 15-18km in diameter. Following impact events, compressed crust relaxes (Melosh, 1989) with relative size of linear features remaining consistent.

Both simple and complex craters are susceptible to filling by volcanic material. Most mare deposits are found on the nearside. Far-side craters are less likely to fill due to thicker crust (Heather and Dunkin, 2003). Impact crater diameter directly correlates with the volume of melt generated at impact and the resulting melt flow morphology (Lev et al., 2021). Complex craters transition to basins around 50-80km in diameter (Williams and Zuber, 1998). Inner central peak rings exhibit a central positive Bouguer anomaly at crater diameters >200km (Neumann et al., 2015). The South Pole Aitken Basin, found directly on top of the Moon’s geographic south pole, is the largest impact basin known in the Solar System and an example of the extent of the Moon’s cratering. As crater diameter increases, so does morphological complexity, while the depth of the crater slows in growth (Williams and Zuber, 1998, Cintala and Grieve, 1998).

2.2: Interior Characteristics of Craters

Lack of data hindered late 20th century research into interior topography. Only one side of the Moon was available for terrestrial observation, and what was visible depended on the technology available. Clementine launched in 1994, returning nearly two million images in the visible and infrared, along with a laser altimeter to create the first global topography map (Hiesinger and Head, 2006). With the launch of each new lunar probe, surface resolution improved enough to characterize crater interiors and map geomorphology, first at 200m/pixel (Hiesinger and Head, 2006), then at 0.5 m/pixel (Zanetti et al., 2011, Robinson et al., 2010), and now with some regions at 0.005m/pixel (Guo et al., 2021), revealing features not previously visible (Carter et al., 2012). Today the clearest global topography map has a lateral resolution of ~100m/pixel from the LRO (Jaumann et al., 2012, Robinson et al., 2010).

Analyses of stereo and altimetry data gathered on recent missions such as LRO and Kaguya Laser Altimeter (LALT) have substantially improved our understanding of lunar topography and allowed for in-depth analysis (Fig. 2). The LROC (Lunar Reconnaissance Orbiter Camera) is the first camera to provide detailed topographical information at a variety of incidence angles, revealing linear features previously unknown (French et al., 2015), and the Mini-RF radar onboard LRO discovered various impact melt features (Carter et al., 2012). Some features of the lunar surface were predicted prior to discovery, such as rougher impact melt terrain predicted by LROC, but were not determined until the launch of Chang'e (Carter et al., 2012, Guo et al., 2021).

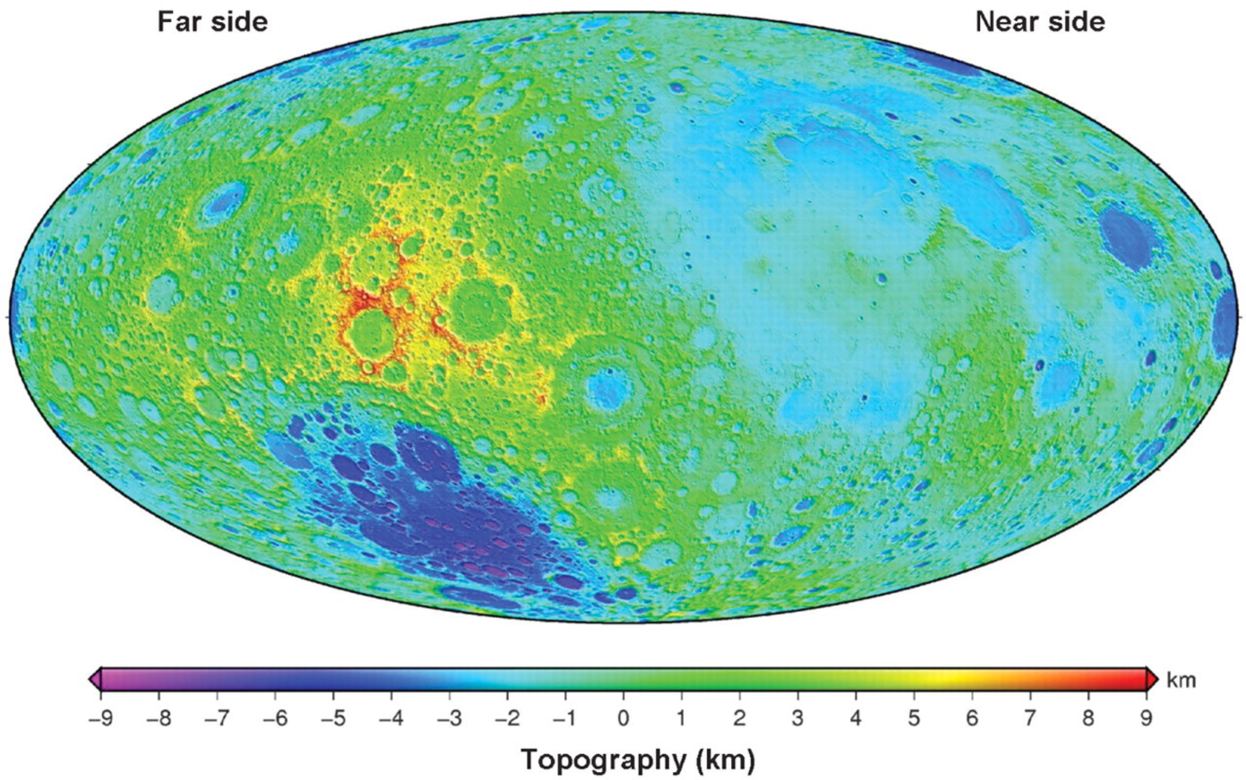

Figure 2: Global topographic map of the Moon. Taken with Kaguya's Laser Altimiter (LALT). Image Credit: Araki et al., 2009

Tectonic and degredational features relate to both impact and volcanism (Cai and Fa, 2020). They are manifested through extensional and compressional features such as faults, graben (landforms caused by normal faulting), scarps, dikes, and wrinkle ridges, though the latter are more prevalent in volcanically filled craters (Bandfield et al., 2011). These features form after melt solidification due to stress caused by deformation. Mare materials create troughs and rilles through extensional stress on crater edges (Jaumann et al., 2012). When the Moon shifted from overall extension to a regime of contraction, rilles became less commonplace, while wrinkle ridges experienced a period of formation (Solomon and Head, 1979). Graben formed in mare-filled craters are on average significantly smaller than highland graben (French et al., 2015). An interconnected global system of lobate scarps indicates recent tectonic activity, although the exact age of these features is currently unknown (Watters et al., 2019). Topography of craters may influence the orientation and appearance of cooling fractures in impact melt-filled craters (Xiao et al., 2014).

Erosion on the Moon greatly alters morphological features of both mare and impact melt-filled craters. A morphologically fresh crater will have distinct features at small scales. The Moon’s features degrade due to micrometeorite collisions forming a regolith over the surface. Regolith generation occurs over time through bombardment of microscopic iron meteorites (Lucy et al., 2006) as well as space weathering from solar wind (Denevi et al., 2014). All surfaces on the Moon have a layer of regolith, where the older surfaces have thicker layers. Topmost layers of regolith are more eroded than bottom layers, due to exposure to space weathering (Wu et al., 2019). The regolith layer softens and erases small-scale features on the lunar surface. Young craters have thinner regolith and thus features are more pronounced and identifiable (Jaumann et al., 2012, Lucy et al., 2006, Campbell et al., 2010). Accordingly, older craters may have distinguishing features erased by erosion over time. Small-scale roughness is dependent on the rate of erosion and regolith formation (Kreslavsky et al., 2013).

Interior crater morphology is dependent on the type of melt fill, as well as previously mentioned crater size, erosional, and deformation processes. Complex craters gain features as diameter increases (Fig. 3), such as central peaks (Smith, 1976, Jaumann et al., 2012), well-developed ejecta, and melt pools (Jaumann et al., 2012). Melt pools are more common in large craters and basins, while craters <10km in diameter have lithified veneers (Lev et al., 2021). Central peaks are mountainous points at the center of an impact crater reaching upwards of thousands ofkm in height. Peaks begin to appear at sizes greater than 18km (Jaumann et al., 2012) and over 50% of craters above 30km in diameter have a central peak (Smith, 1976). Central peaks erode as regolith covers the crater interior. The appearance of ejecta and melt pools inside impact craters relies on pre-existing topography the crater overlays (Heather and Dunkin, 2003, Lev et al., 2021) and form during excavation of the crater. Pre-existing topography can alter the flow of ejecta, preventing mixing between debris and increasing the likelihood of flow solidifying (Bray et al., 2018). Evidence of melt flow solidifies in relatively low-lying topographic areas following crater formation. Impact melt resting on terraces on crater rims may pond or flow down into the crater floor (Ashley et al., 2012, Dhingra et al., 2017), indicating free-moving melt during crater formation, a feature unique to impact melt-filled craters. Shaking during crater formation significantly alters flow of impact melt before solidification (Kreslavsky and Head, 2012). Other features visible in impact melt-filled crater interiors include preserved channels of melt flow and flow lobes that indicate individual sections of melt moving independently (Lev et al., 2021), collapse pits (Robinson et al., 2012), large boulders or clusters of boulders that rest at smooth elevation following emplacement, and mounds of impact melt overlaying pre-existing topography (Zanetti et al., 2011). The relatively higher albedo of impact melt-filled craters may be attributed not only to the same relative chemistry of surrounding highlands, but also due to large blocks and boulders that appear bright and therefore rough (Jaumann et al., 2012). Some mounds appear to have fractured as impact melt solidified on top of pre-existing topography (Ashley et al., 2012). Impact melt flows appear low in viscosity (Ahsley et al., 2012, Carter et al., 2012) and solidify slowly. At a lower resolution, interior floors of impact melt-filled craters appear ponded or smooth, however at meter and millimeter scale the surface is rough (Guo et al., 2021) with mounds, boulders, and fractures. Hummocky and lineated facies are most identified in impact melt-filled craters (Plescia and Robinson, 2019). Solid debris also appears as well as impact melt from crater walls post slumping (Xiao et al., 2014).

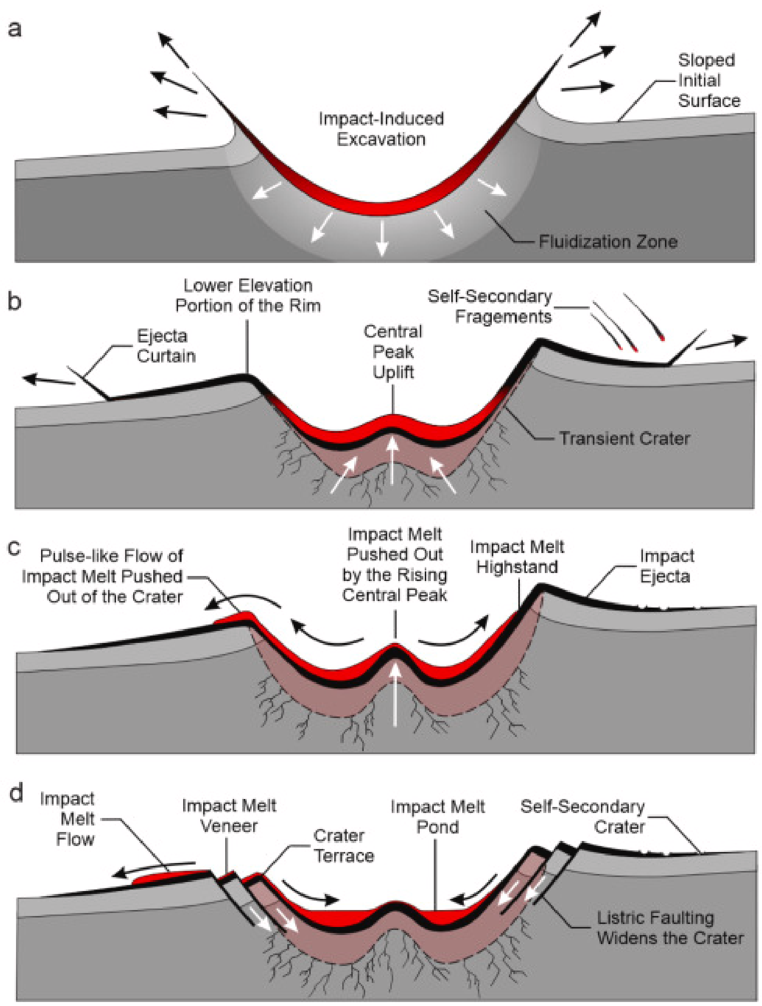

Figure 3: Schematic illustration of one potential impact melt emplacement process associated with a complex crater on the Moon (Lev et al., 2021)

The distinguishing feature of mare volcanism is dark albedo relative to the surrounding highlands. While distinctive pre-existing topography dominates impact melt-filled craters, mare volcanism covers up any topography or previous melt, though pre existing topography does indicate the thickness of mare. As mare rises up from beneath the lunar crust, magmas fill in the crater floor and even superposed craters that formed on top of the main basin (aka embayed craters). For the purposes of this paper, the term “embay(ed)” is used to refer to buried or partially buried impact craters inside larger craters (O’Rourke et al., 2014). Embayed craters predate any fill, but are obliterated in any impact melt forming cratering event. In contrast, mare flow preserves the original topography under the surface. Only the highest points of elevation in preexisting craters remain visible in volcanically filled craters, such as central peaks or crater rims. The extent of filling is determined by the volume of volcanic melt generated at the time of fill. Extensional stress at the edges of volcanically filled impact craters is caused by the volume of material filling the crater (Jaumann et al., 2012). Several characteristics of volcanically filled impact craters share a commonality with slow-moving terrestrial lava flows, such as kipukas (elevated terrain embayed on all sides by mare) (Runyon et al., 2019), volcanic complexes and dark halo craters (Head, 1976), though with some differences, such as erosional channels (Bray et al., 2010). Mare volcanism trends towards low lying topography such as the interiors of impact craters (Head, 1976) and fill until the volume of mare has depleted, sometimes leaving parts of the original crater visible. This filling mechanism also leaves volcanically filled crater floors smooth at small scales (Cai and Fa, 2020), while appearing rougher at large scales alongside a lower albedo. Cryptomaria are mare pools obscured by higher albedo deposits, such as crater ejecta (Antonenko et al., 1995). Mare unable to be identified by lower albedo can be determined by other factors such as location of nearby mare deposits or basin topography (Antonenko et al., 1995).

2.3: Mineralogical Properties of Impact and Volcanic Flows

Modern spectroscopic research on the lunar surface debunked hundreds of years of work into the search for change to its surface (Wood, 2018). Chemical analyses were limited by on samples brought back from the Apollo and Luna missions (Nagaoka et al., 2021, Gillis et al., 2004) until lunar meteorites were recgonized and spectral data could be obtained from the Galileo (Hiesinger and Head, 2006), Lunar Prospector, and Clementine missions (Binder, 1998, Gillis et al., 2004). Spectroscopy from these missions was calibrated using samples ground truth from lunar (Nagaoka et al., 2021) providing insights into the internal composition of the Moon in places where samples could not be taken (Hiesinger and Head, 2006). The composition of materials on the Moon is critical in determining their origins. Ejecta deposits may differ in composition due to the bombastic origin of impactors (Guo et al., 2021). Composition of specific areas may be determined regardless of surface maturity thanks to improved algorithms (Lucey et al., 2000).

Higher albedo typically indicates impact melt mixed in or entirely comprising an area (Hawke et al., 1999). Impact melt remains liquid for months or even years (Heather and Dunkin, 2003) with a high initial temperature (Jaumann et al., 2012, Runyon et al., 2019) even reaching as high as 1770°C (Xiao et al., 2014). Solidified melt and superposed regolith may retain higher relative temperatures for even longer periods

(Bandfield et al., 2011). Impact melt material is spectroscopically similar to the felsic highlands (Belton et al., 1994), which is distinguishable by relatively low concentrations of FeO (Guo et al., 2021). It must be noted that highlands and impact melt are not the same, and in fact there are pristine highlands with no impact melt mixed in (Hiesinger and Head, 2006). Visible upper crust deposits are typically determined to be impact in origin, including the Aitken Basin, which is composed of upturned crust from deep beneath the surface (Petro and Pieters, 2004). Highland and impact melt materials are also characterized by low concentrations of Th (Petro and Pieters, 2004, Guo et al., 2021). Samples collected from the Apollo landing site originated from impacts, and therefore any spectral imaging with a similar composition can be determined as such (Head et al., 1993). Despite possibly being different in composition to the lunar surface, impactors do not substantially contribute to the overall composition of impact melt due to their relatively small size. However, impact melt contributes to the lunar regolith over its entire surface (Bandfield et al., 2011). Impact melt is also lower in Ti.

Mare basalts, in contrast to impact melts, are rich in TiO_2 and FeO (Guo et al., 2021, Neish et al., 2014). The distinction between Ti-poor highlands and impact melt and Ti-rich basaltic mare material is important for distinguishing the two, as well as for classifying individual mare basalts. Early mare volcanism is Ti-rich, decreasing with each subsequent flow (Head, 1976) and Fe (Thesniya and Rajesh, 2020). More recent flows are low in Ti and enriched in Mg and Ca. Mare material is basaltic, which means it is rich in augite or other dark-coloured pyroxene minerals. This darkness provides the mare with its distinct low albedo. In some cases, the difference in relative albedo cannot be determined solely on the visual spectrum, and what was believed to be mare material is actually shocked impact melt (Hawke et al., 2010). In areas with a presumed thinner crust, such as the Apollo landing sites and other large basins, Ti content is often higher than the surrounding areas (Greeley et al., 1993). Enriched levels of TiO_2 in mare deposits may obscure subsequent Ti-poor impact melt flows (Neish et al., 2014). Increased levels of CaO are also common. Basaltic mare deposits are low in Th (Guo et al., 2021). Mare volcanism is also low in Al_2O_3 and have higher CaO/Al_2O_3 ratios compared to surrounding highlands (Hiesinger and Head, 2006). Areas high in TiO_2 have the same optical distortion as space weathering, in that both reduce overall albedo (Wu et al., 2019), suggesting that previous samplings of the lunar surface were not as pristine as once thought. All of the chemical imbalances are a direct result of the evolution of the lunar interior. The near and farside of the Moon differ in concentration of radioactive heat sources. The nearside experiences a higher concentration in a region known as the Procellarum KREEP Terrane (PKT) (Laneuville et al., 2013). Mare basalt on the nearside flooded basins in or adjacent to this terrane. Evidence of molten lower mantle (Khan et al., 2014) suggests a molten mantle earlier in the Moon’s history. High temperature magma from the mantle would rise up to the surface and cool quickly. As basaltic material is the earliest to form, it would be the most prevalent in a rapidly cooling exposed mantle.

Global estimates for the range of FeO and TiO_2 have remained consistent as new data were added by theLP and Chang'E-1 missions (Gillis et al., 2004, Yan et al., 2012) at 0–21.0 wt% and 0–9.5 wt% respectively, however data from Clementine suggest areas with the most abundance may have a different wt%. Variations in age and abundance of Ilmenite ($FeTiO_3$) affect visual properties of mare deposits (Campbell et al., 2010) and may account for some of these irregularities (Yan et al., 2012).

Individual surface units have unique regolith temperatures (i.e. the surface temperature of the thin layer of dust and debris on top the lunar surface) and rock concentration values (areas with actual rock versus a layer of regolith) that distinguish between mare and impact melt material. Regolith layers are highly insulating while solid rock is highly conductive (Bandfield et al., 2011, Roelof, 1968). The resulting temperature difference can be easily observed by infrared cameras such as those onboard LRO. While higher temperatures do not necessarily indicate higher rock concentrations, viewing varying concentrations of regolith and rock via infrared illuminates differences between impact and mare surfaces. Regolith with higher temperatures are present in rims, walls, and crater floors (Bandfield et al., 2011). Rock abundance studies on the Moon have been limited to only observing the fractional area of surface covered by rocks >1m in diameter (Li and Wu, 2018), making detailed conclusions difficult. However, on a broad scale it is fair to say that rock concentration values are lower in mare deposits, crater floors, and distal ejecta (Bandfield et al., 2011).

2.4: Age Stratigraphy

The history of the Moon is separated into several distinct eras, however this thesis focuses on the time before and after heavy bombardment, while only referring to cratersusing relative age (if they are older or younger than other craters). The era of heavy bombardment, ~4Ga, was marked by numerous asteroid impacts. That formed a substantial number of craters, many of which are still visible. Techniques for dating craters and flood material inside craters date back to before the Apollo missions, with age estimate methodologies evolving over time. Primary methods for dating the lunar surface include crater counting, crater degradation levels, and age-dating of returned samples (Hiesinger et al., 2003, Nagaoka et al., 2021), all of which can determine the relative ages of areas on the Moon. Crater counting follows the logic that an older crater has more time to be obscured by superposed impacts called secondary craters (Stopar et al., 2014). By the 1960s, general consensus on the starting era for the Moon's volcanic activity was estimated to be approximately 4-3.8 Ga at the end of heavy bombardment, with most basaltic eruptions occurring in the first billion years and petering out around 2.5Ga (Head, 1976). More recent studies place the end date of lunar volcanism more and more recently (Hiesinger et al., 2003, Singh and Srivastava, 2020), with the current estimate to be around 1 Ga. Determination of the exact date varies by model.

The law of superposition implies that any crater or feature superposed on top of the underlying crater must be younger (Runyon et al., 2019). Certain younger craters may contain self-created secondary craters, superimposed on top of the primary crater (Shoemaker, 1962, Plescia and Robinson, 2019). More recently developed techniques include observing optical maturity (Denevi et al., 2014), which is a measure of regolith development and space weathering affecting the surface. A more weathered surface with thicker regolith is optically more mature, often appearing as a darker albedo. Hence older impact melt-filled craters are classified as volcanically filled (Ashley et al., 2012, Plescia and Robinson, 2019).

Because the beginning of mare volcanism on the Moon coincides with the end of heavy bombardment, the first volcanic flows on the Moon are buried under ejecta (Hiesinger and Head, 2006). Ti-rich basaltic flows flooded the eastern nearside at 3.5 Ga, with previously mentioned surface-wide subsequent flows decreasing in Ti contents by 3.5-3.0 Ga (Head, 1976). These thin layers sequentially are relatively homogenous, and the Ti gradient is only visible over large periods of time (Greeley et al., 1993). While volcanic activity is now believed to have continued into the Copernican, most visible maria were emplaced by 1.5 Ga (Hiesinger and Head, 2006), so any volcanically filled craters are likely older than that date. Pre-Nectarian craters such as Von Kármán were flooded by mare basalts during the Imbrian and Nectarian periods (Guo et al., 2021). Because volcanic material flows into low-lying topography, any previous crater topography is buried under the volcanic flow. Currently the Moon is volcanically inactive because the interior cooled.

Along with volcanic activity, crater formation slowed over time. However impact craters are independent of geologic activity on the Moon, so they can occur at any time; some are younger than mare fill. They sometimes cover mare deposits with ejecta or regolith (Guo et al., 2021), creating cryptomaria. Instruments that remotely sense characteristics of impact and volcanic material are crucial for differentiating between the multiple materials that may exist in an old crater. For example, young impacts into pre-existing craters may expose cryptomaria, which appear as dark-haloed craters (Bell and Hawke, 1984). Younger craters are typically rougher than older craters, and thus small-scale roughness can be interpreted to indicate more recent activity, while kilometer-scale features suggest older events (Guo et al., 2021). Impact melt emplacement duration depends on individual crater conditions and can be used to estimate the age of craters (Lev et al., 2021). Younger, more pristine craters exhibit preserved impact features such as bright rays, stretching tens to hundreds ofkm across the lunar surface. These are created from ejecta at the moment of impact (Hawke et al., 1999). One example is Giordano Bruno, a crater with rays extending into nearby craters visible under Clementine's multispectral imaging. Because these rays are composed of small-scale features across the lunar surface, they fade relatively quickly under layers of regolith or through space weathering. craters older than 1 Ga typically do not have visible rays. Other features unique to younger craters include higher temperatures in the central uplift and floor, as residual heat from the formation slowly dissipates (Jaumann et al., 2012). This correlation between craters and temperature falls off at smaller scales (Bandfield et al., 2011). Another value that falls over time is the d/D ratio because erosion wears away at the topographic extremes in lunar craters and regolith covers the floor.

2.5: Relevance of this Thesis

Understanding the history of lunar exploration and research gives context to and justifies this study. Limitations of previous studies led to conclusions or findings that were subsequently updated to influence more modern research. By examining the past century and beyond, it becomes clear why certain conclusions were drawn (i.e., the volcanic theory versus impact theory for impacting). With each successive probe mission, a review of previous studies and determining their validity is of vital importance. If studies based on previous knowledge no longer hold up, a more likely theory must be proposed in its place. Understanding the timeline of events also justifies gaps in research. For example, a gap between missions to the Moon explains an absence of topographical research prior to the 1990s (Head and Wilson, 1991, Head, 1976). Previously mentioned improvements in technology correspond to large influxes in research regarding the topics new missions were able to cover (Fig. 4) (Robinson, 2010, Jaumann et al., 2012).

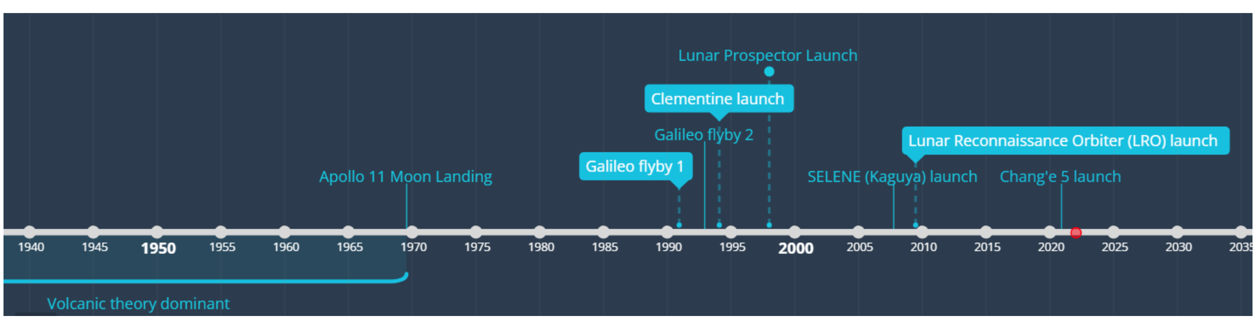

Figure 4: Timeline of major lunar missions discussed in this paper. All time pre-1969 had no samples from the lunar surface, and volcanic theory was the dominant theory. Current day (2022) is marked in red.

All of this information is crucial to differentiating between impact and volcanic melt on the surface of our Moon and other bodies. Unlike on some other planetary bodies, volcanic material on the Moon is easily distinguishable by its lower albedo, which is noticeably dark surface material relative to the lighter felsic lunar crust. Volcanically filled craters suggest the importance of volcanism in lunar history, best seen in the basaltic low albedo mare that covers the nearside (Head and Wilson, 1991). Classification of individual craters relied on specific features, such as the aforementioned dark albedo, only for the crater to later be reclassified (Ashley et al., 2012). Comparing and contrasting the two fill types to begin to create a comprehensive morphological guide, allows fill type to be determined through means beyond just a handful of features. Because lunar craters have been heavily studied and imaged, there are many sources of data available to identify key traits in each fill type.

Individual features of crater interiors cannot definitively prove one way or another which type of melt is present. Previous attempts have been made to create a comprehensive guide to differentiate between volcanic and impact melt (Jaumann et al., 2012). However, individual features may be present in specific craters regardless of fill because their appearance is more dependent on other factors such as location, size, or age. This thesis seeks to examine craters in which these factors vary, in order to determine whether fill type influences the presence or absence of certain features considered universal in one fill type. If a characteristic is determined not by interior composition, but rather by some other factor, then it cannot be considered a diagnostic feature for determining the origin of craters moving forward.

If certain features are truly dependent on the origin of melt material, then this paper benefits future studies on our Moon. Moreover, should certain factors play a role in morphological characteristics, then this information can be applied beyond one body. Features that appear or disappear due to age, for example, can be applied to bodies in our Solar System with older surfaces, or can even determine that a certain feature is older or younger than previously estimated. Surfaces with similar origins or compositions to the Moon may also apply this research when examining topography. The large quantities of data available for the Moon serve as excellent points of reference for bodies with considerably less data. Global high-resolution images, for instance, require recent and long-lasting missions that sometimes are lacking. However examination of similarities between Venus and the Moon may yield a comparison and therefore possibility of similar variations in melt deposits, as well as on other bodies.

3: Methods

To characterize and analyze the features of volcanic and impact melt-filled impact melt-filled craters, this thesis looks at eight different craters on the lunar surface, all with a diameter approximately >60km. Geologic mapping and digitization of features was completed using the JMARS Geographic Information System (GIS) software package (Christensen et al., 2011). Nested data were used during the mapping process by labeling features of note at a set scale, then zooming in and repeating until the features measured approximately <5km in either the vertical or horizontal direction. While some areas of the Moon are now visible at the meter and millimeter scale (Guo et al., 2021), this is not the case across the entire surface. Thus, this thesis uses the smallest scale that is globally available. The sharpest global resolution can be found primarily using the Lunar Reconnaissance Orbiter Camera (LROC) Wide Angle Camera (WAC) Global 100m/px dataset (Robinson et al., 2010). To see at a smaller scale, LROC Narrow Angle Camera Left/Right (NACL+NACR) images were rendered as stamps. These image pairs provided 0.5 meter-scale panchromatic images over a 5km swatch. The available LROC NAC data were filtered to show only images with incidence angles (angle at which the camera was pointed) ranging from $70° \mp 10°$ to emphasize the morphology of features. This angle range was chosen because it allowed for the best view of crater features, and keeping everything within 10° allowed for a smoother-looking mosaic. This allowed for better visibility of the smaller features. Specifically, any possible feature of interest at the 100m/px scale was loaded the stamps of that area for a clearer image. This was not always possible, as not every feature had data at those incidence angles, resulting in gaps and mismatches in the final rendering of LROC NAC image data. Furthermore, some features appeared in one position on the global dataset, while in another position on the LROC stamps. This occurs due to georeferencing–turning a digital image into real world coordinates. The images are 2D being fitted onto a 3D globe, and as such different angles result in different configurations (Christensen et al., 2011). To examine ejecta, the LROC WAC 643 nm Normalized Reflectance (Boyd et al., 2013) were loaded. The 643 nm WAC mosaic is a mosaic of the 643 nm reflectance band and emphasizes differences in albedo compared to morphology. When mapping the rim and fill sections of the crater, the Unified Geologic Map of the Moon was overlaid on top of the LROC WAC, however the global dataset superseded the map (Fortezzo et al., 2019). Larger boundaries were given thicker lines and a unique color, in order to differentiate areas of interest. Small features were all one uniform color. This mapping was done for archival purposes, and the colored outlines will only be used in this paper should they be of interest.

Other data sets used included the Clementine UVVIS Mineral Ratio (Tompkins and Pieters, 1999). This map enhances color differences caused by surface mineralogy and maturity. Volcanic and impact materials are typically of differing age and composition, because impact material is composed of both the target and impactor's original composition, while lunar volcanism is basaltic. The older lunar highlands and basins are depicted as dark red, while younger surfaces are blue. Similarly, the Fe-rich basaltic maria contains varying levels of Ti. Lower Ti is portrayed in yellow and orange, while higher titanium appears blue. Superimposed are materials from basins and craters of various ages, with dark red and blue in ancient basins and bright blue on crater rays of younger craters (JMARS). Another Clementine map is the UVVIS/FeO Abundance, which measures iron concentration, which occurs both due to chemical composition and optical maturity. Optical maturity refers to trace amounts of iron deposited over time, causing the surface to darken. A redder color indicates more Fe, and therefore older surface.

The mapping and analysis of the craters was done over two periods of time in two different locations (Flagstaff and South Hadley). Thus, certain renders may be of differing resolution because of the limitation of the computer available. Five of the craters were mapped in Flagstaff, and the data was transferred over onto a new computer during the second period. The first computer had more processing power. The second had less processing power and was at times unable to render images of the lunar surface. This caused significant delays in work.

4.1: Mare-filled Crater Results

Joliot (25.922°N, 93.454°E) is a crater 172km in diameter (Fig. 5). It consists of a mare unit south of the peak, and a large, steep crater rim. Just west of the central peak is a large embayed crater, or perhaps two embayed craters overlapping, about 38km in diameter (Fig. 5a). The rim of the embayed crater is absent to the southwest. Joliot has a degraded central peak that appears almost hand shaped, with outreaching prongs, likely the result of erosion over time. At the southern edge of the mare is a misshapen embayed crater. Joliot's wall is not terraced (having levels with smooth fill) and severely degraded. However, in the north there is what appears to be a second level. It has the same albedo as the wall, unlike the darker albedo of the fill. To the southwest is a wrinkle ridge approximately 34km long (Fig. 5b). This ridge runs from the edge of the large embayed crater into the mare. There are no linear features on the wall or rim. The crater floor seems to be covered in a layer of ejecta superimposed on the crater floor. Joliot's albedo appears significantly darker than its surroundings, but not as dark as the other volcanically-filled impact craters'.

Under the UVVIS Fe/O ratio dataset (instrument that measures iron content), the crater appears to have a blue central peak, surrounded by a ring of yellow. This means that Joliot's central peak and other non volcanic material is low in iron, while the volcanically filled floor is higher in iron. In comparison, under the Clementine mineral ratio the crater appears to be a mixture of red and blue with pockets of green scattered throughout the crater.

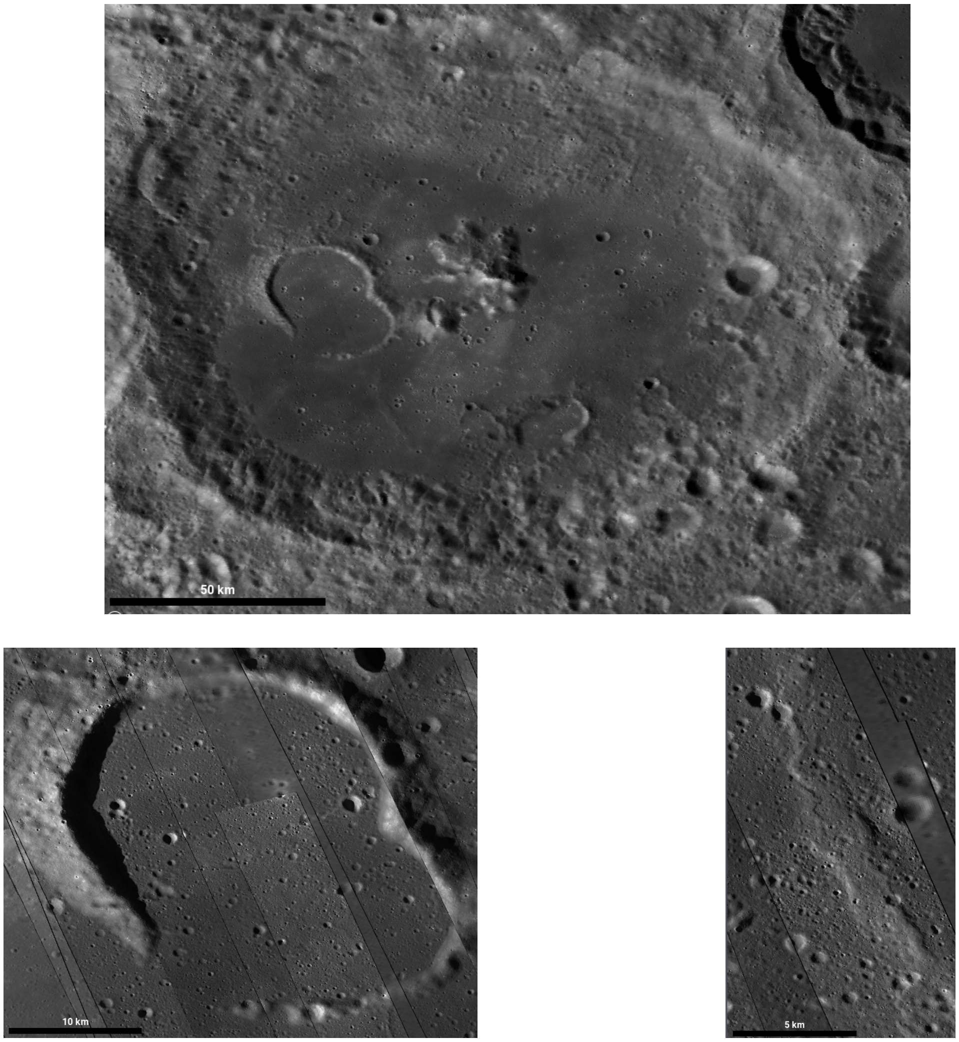

Figure 5: Joliot, 25.922°N, 93.454°E taken with LROC WAC. Joliot is a volcanically-filled impact crater that is covered with superposed ejecta due to several surrounding, younger craters. Its rim is heavily degraded as is the central peak, indicating that the regolith is thick and smoothed over much of the terrain. Figure 5a: 26.09°N, 92.251°E taken with LROC NAC. A large embayed crater in Joliot. The lower left corner of the rim is missing, likely buried beneath the volcanic fill due to its lower elevation. The remaining crater is at a higher albedo than the fill. Figure 5b: 24.828°N, 92.431°E taken with LROC NAC. A wrinkle ridge in Joliot running from the largest embayed crater into

the volcanic fill. It is approximately 34km long and is covered in secondary craters and ejecta.

Tsiolkovskiy (-20.383°N, 129.808°E) crater is 184km in diameter (Fig. 6). Compared to the other far-side mare craters, Tsiolkovskiy's albedo is significantly lower than the area surrounding it, causing the crater to stand out prominently. The crater rim remains mostly whole, with a steep wall. Linear features are sharp cliffs with shadows due to the incidence angle, indicating terracing. The wall is terraced into two levels. One level drops a remarkable 3500km to the second level, before dropping another 1500km to the crater floor. There are no definitive embayed craters visible. A few linear features are clustered close together mostly to the north. To the north is an area that is the same albedo as the wall and surroundings but at the same elevation as the floor fill. Most of the linear features occur at this boundary, with lengths approximately <15km. Across the crater floor are small areas of elevation with a different albedo than the surroundings (Fig. 6a). Tsiolkovskiy also has a prominent central peak. Surrounding the peak are a series of secondary crater clusters. Tsiolkovskiy exhibits a clear boundary between the basaltic floor and remaining terrain, both under the LROC images as well as the UVVIS and Clementine maps. The Clementine mineral ratio (which displays a ratio of the mineral composition, and certain types of geology indicate age) shows Tsiolkovskiy as high-titanium blue at the rim and central peak, while the mare is a lower-titanium yellow-green. The boundary is most prominent under the UVVIS Fe/O dataset, where the crater floor is a neon orange, indicating high levels of iron, and the central peak and rim are blue with much less.

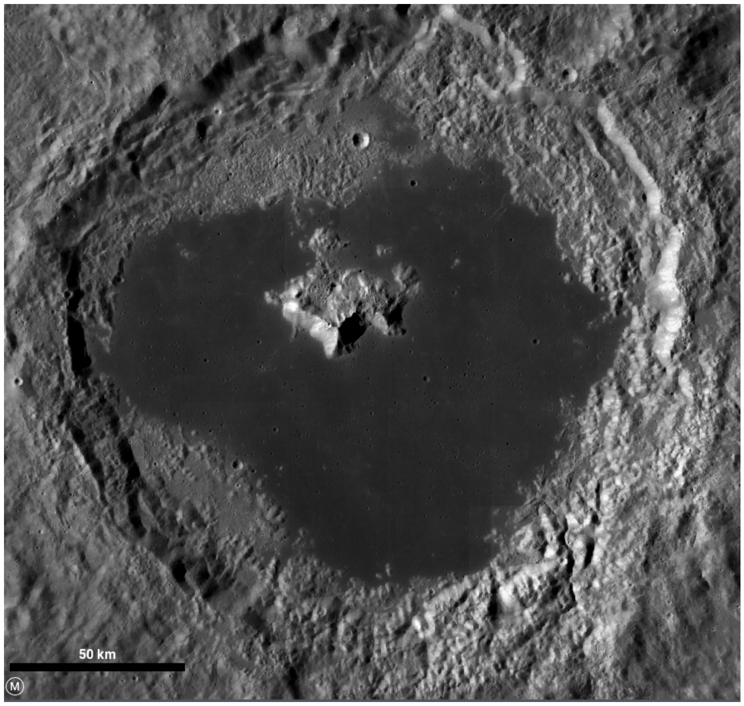

Figure 6: Tsiolkovskiy, -20.383°N, 129.808°E taken with LROC WAC. Tsiolkovskiy is the youngest volcanically-filled impact crater observed in this study. It also contains the highest concentration of iron of all the craters, as evidenced by its significantly darker albedo. Tsoilkovskiy has no embayed craters.

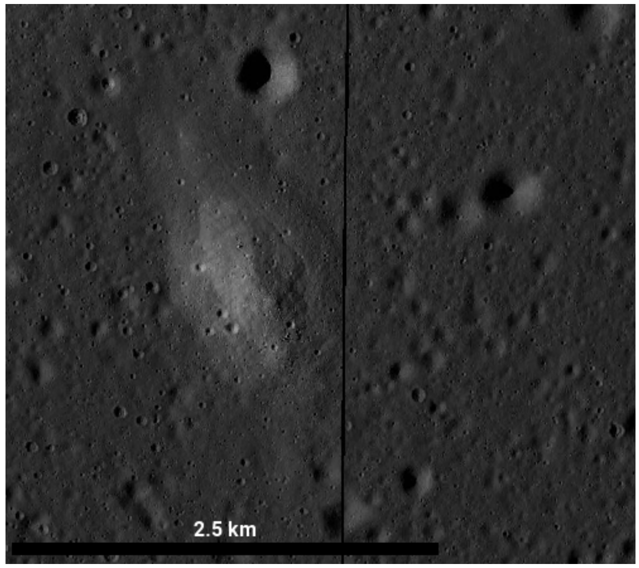

Figure 6a: -19.578°N, 129.14°E taken with LROC NAC. An example of the small mounds scattered across Tsiolkovskiy, as well as several secondary craters. The juts are small increases in elevation with the same albedo as the initial terrain, suggesting that these are part of the central peak or other crater materials that were present prior to volcanic infill.

The Jules Verne (-34.772°N, 146.997°E) crater is 143km in diameter (Fig. 7). Its eastern side has several craters both inside the crater and partially superposing it, including a large one on the rim with ejecta spilling into the main crater. These superposed craters range from 5 - 32km in diameter. The largest of these craters creates a sharp increase in elevation relative to the floor, after reaching a peak drops 3000km into the crater. The superposed crater destroyed any crater rim, as aside from the aforementioned peak there is no change in elevation into the floor aside from other craters. The west has smaller craters, and it also contains two embayed craters. One of these craters has a linear feature tracing out where the crater rim would have been, and ending in what appears to be a pool of material (Fig. 7a). The other embayed crater has a small remaining central peak. The east side of Jules Verne is separated by a massive scarp >100km long (Fig. 7b). Jules Verne is different from the other two craters in that linear features occur both on the low albedo mare as well as the rougher material at about the same level. Jules Verne also has a much shallower slope for a crater rim, aside from places where superimposed craters destroyed the preexisting rim. Jules Verne is a yellow-orange under the UVVIS/Fe abundance dataset, indicating high iron. While the rim of the crater under the Clementine mineral ratio appears to be the same color ratio as the surrounding terrain, the red and blue of an ancient basin, the mare is yellow and green (meaning low titanium).

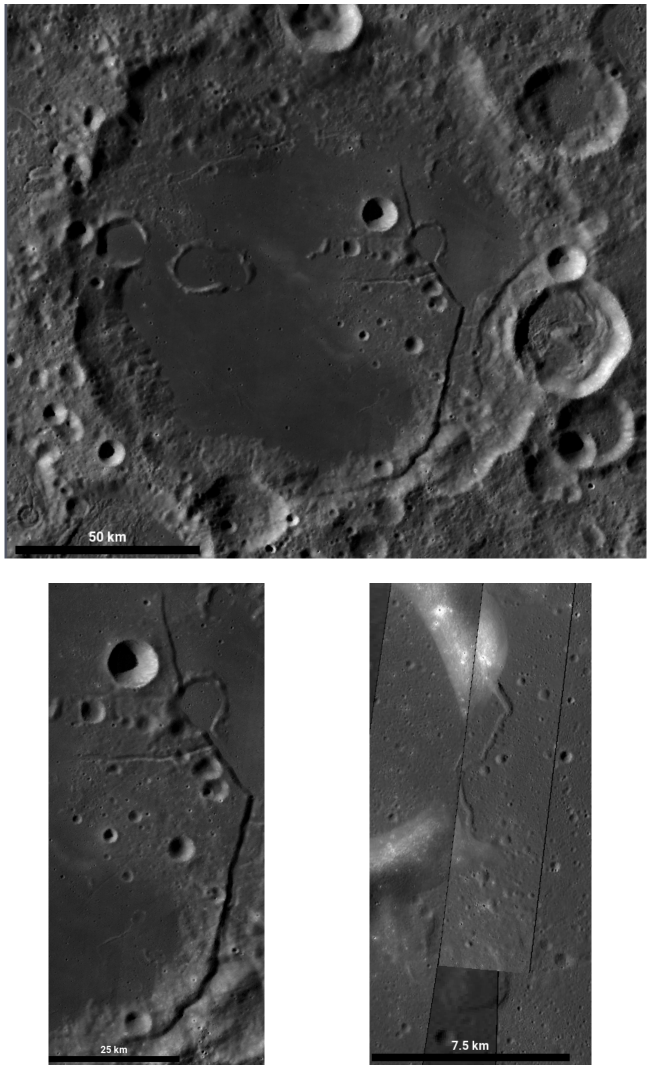

Figure 7: Jules Verne, -34.772°N, 146.997°E taken with LROC WAC, is a volcanically-filled impact crater that is covered in superposed craters. The rim is partially obliterated by these craters. Inside the crater are embayed craters and a large scarp that separates elevation levels. Figure 7a: -34.962°N, 145.329°E taken with LROC NAC. Evidence of flow in one of Jules Verne's embayed craters. The melt material creates a small line that separates the hidden rim of the embayed crater and the rest of the floor. That line pools south into a small pond. Figure 7b: -35.635°N, 148.639°E taken with LROC NAC. Jules Verne's large scarp that cuts across the crater floor. Several secondary and superposed craters can be seen along the edge of the scarp, and flow is smoother in the upper right at lower elevation.

Archimedes (29.717°N, 356.007°E) is a crater that is 84km in diameter (Fig. 8) located in the eastern portion of the Imbrium basin. In the LROC WAC 100 m/pix data set, the albedo of Archimedes is the same as its surroundings, however the basin in which it is located is of significantly darker albedo than the highlands on the north nearside. Upon closer inspection, the albedo of Archimedes proves significantly lighter and covered in ejecta. It is still lower albedo than the lunar highlands. The south and southeast rim of the crater shows two levels to the wall, however all other sides of the crater rim are of a single level before dropping 2km into the bowl of the crater (Fig. 8a). A ring of elevation surrounds Archimedes on all sides, creating two layers of crater rim. The floor of Archimedes is level, with secondary craters pockmarking the surface.

Linear features can be seen towards the north of the crater floor running in a line across the northern half of Archimedes (Fig. 8b). Some sections appear as linear features separate from the overall trend, Other portions of this area are separate individual clusters that appear identical and run along in a dotted line. Other than these features, the floor of Archimedes is relatively featureless. There are no embayed craters and no central peak. Under the Clementine color ratio, Archimedes appears overall similar to its surroundings with two notable exceptions: the floor or Archimedes just slightly bluer than the surrounding mare, appearing green and iron-rich. That green is surrounded by a ring of red significantly brighter than any nearby terrain, reflecting the age of the crater. While the Imbrium basin is a bright orange under the UVVIS/FeO (iron) abundance filter, Archimedes rests in a small pocket of yellow between the

Imbrium and Serenity basins, indicating a lower level of iron between the two. Still, the abundance of iron in Archimedes is relatively high.

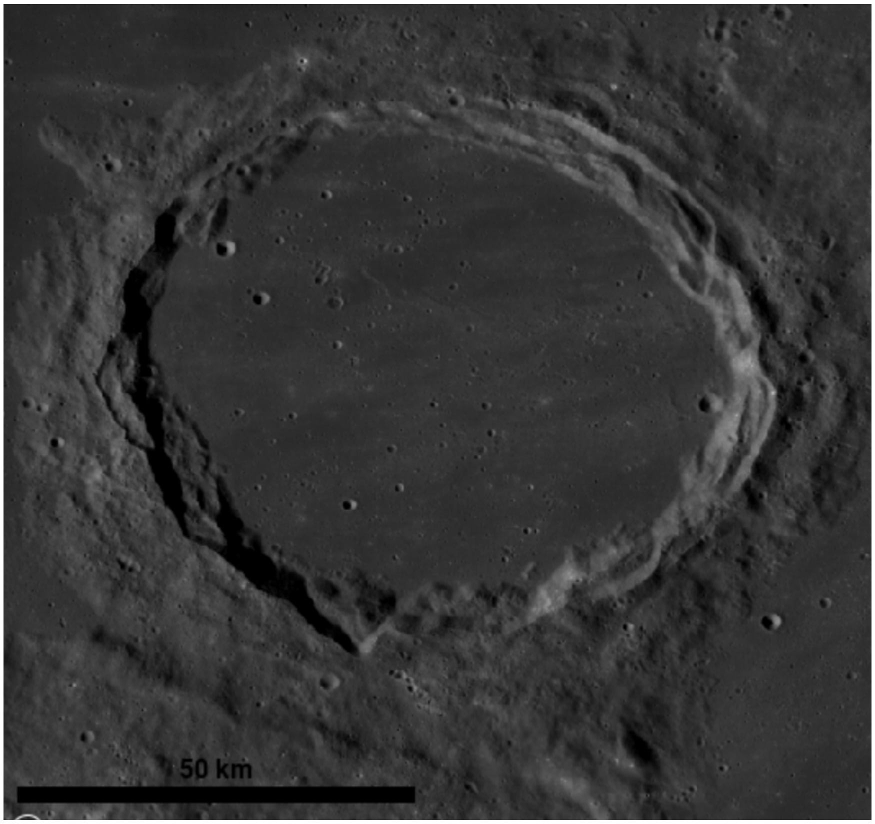

Figure 8: Archimedes, 29.717°N, 356.007°E, taken with LROC WAC. Archimedes is relatively featureless with volcanic fill completely covering the surface of the crater. A ring of debris around the crater rim shows the same albedo as the mare inside the crater due to its location in the Imbrium basin.

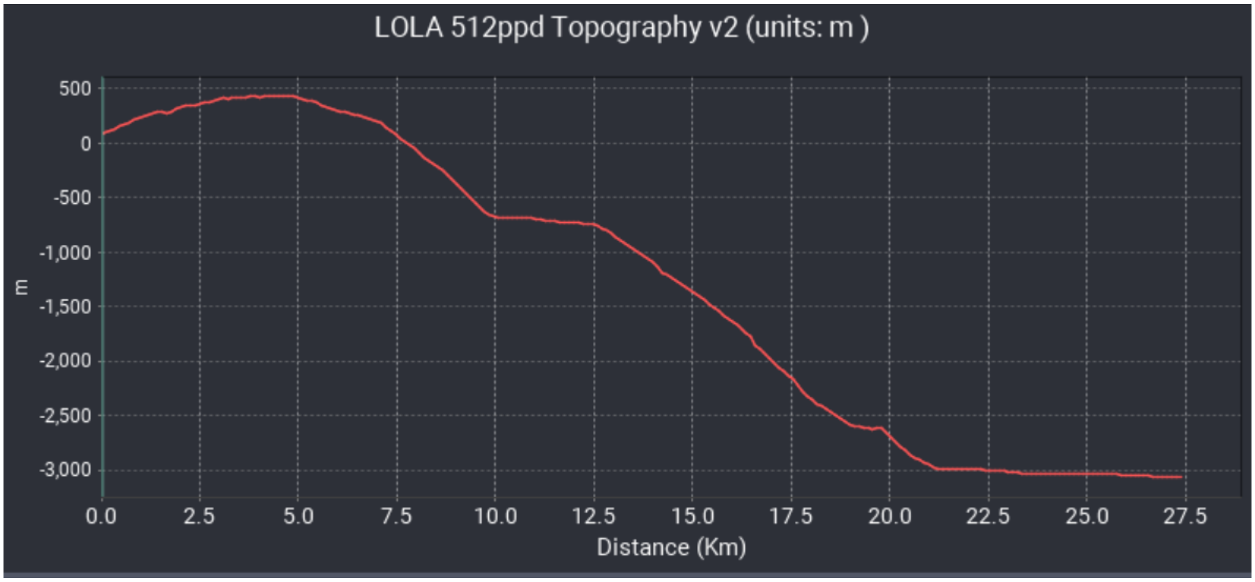

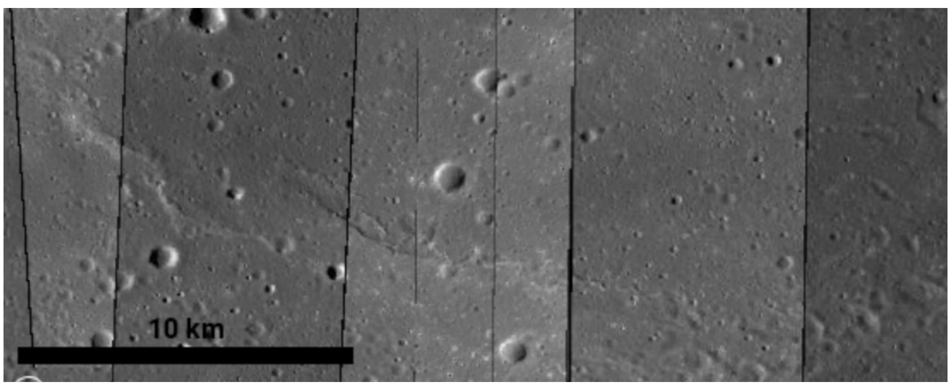

Figure 8a: Elevation chart of the crater rim. Elevation on y axis is in m, while distance measured is inkm. Information gathered from Lunar Orbiter Laser Altimeter (LOLA). There are two distinct levels of the crater rim, indicating a terrace that has heavily eroded. The crater rim is shallowly sloped as it drops 3.5km into the crater floor. Figure 8b: 30.002°N, 356.045°E taken with LROC NAC. A series of smaller linear features forms one larger feature when grouped together, measuring approximately 20km overall. The feature cuts across Archimedes' northern fill.

4.2: Impact-filled Crater Results

Ohm (18.389°N, 246.189°E) is a crater 64km in diameter (Fig. 9). It consists of a rim, central peak, and a floor separated by varying textures. The crater floor appears generally ponded and smooth from a distance, however when zoomed in it is apparent that Ohm is covered in relatively rough (compared to the volcanically-filled impact craters) terrain and linear features. Just southwest of the central peak is an area showing evidence of flow movement (Fig. 9a). The surface of this patch is smoother than the surrounding terrain and pools at the bottom of the central peak, as evidenced by fractures layering on top of one another at the base of the feature. The smooth material is only the base because the feature is covered in small pockets of boulders. In fact, the whole crater is covered in these pockets of boulders (Fig. 9b). The boulders are never larger than a few meters in diameter but cluster together. On this feature, the boulders are clustered in circular formations surrounded by a massive group of boulders. Just east of the central peak are a series of mounds and fractures (Fig. 9c). The mounds are <1km in diameter, surrounded by linear fractures <3km long that radiate from the mounds. Some of the fractures connect mounds together. Ohm also shows fractures at the boundaries between floor and rim. Ohm's rim is terraced, with pools of melt on the east rim. In the northeast, a small pocket of pond exists on the rim. Under the normalized reflectance, Ohm's ejecta extends approximately 385km beyond the crater boundary. These rays are visible under the UVVIS FeO ratio as green overlaying a blue crater to indicate low iron levels, and under the Clementine mineral ratio, a bright teal indistinguishable from the area around it, showcasing the younger rays. It is unclear if this teal also indicates high titanium.

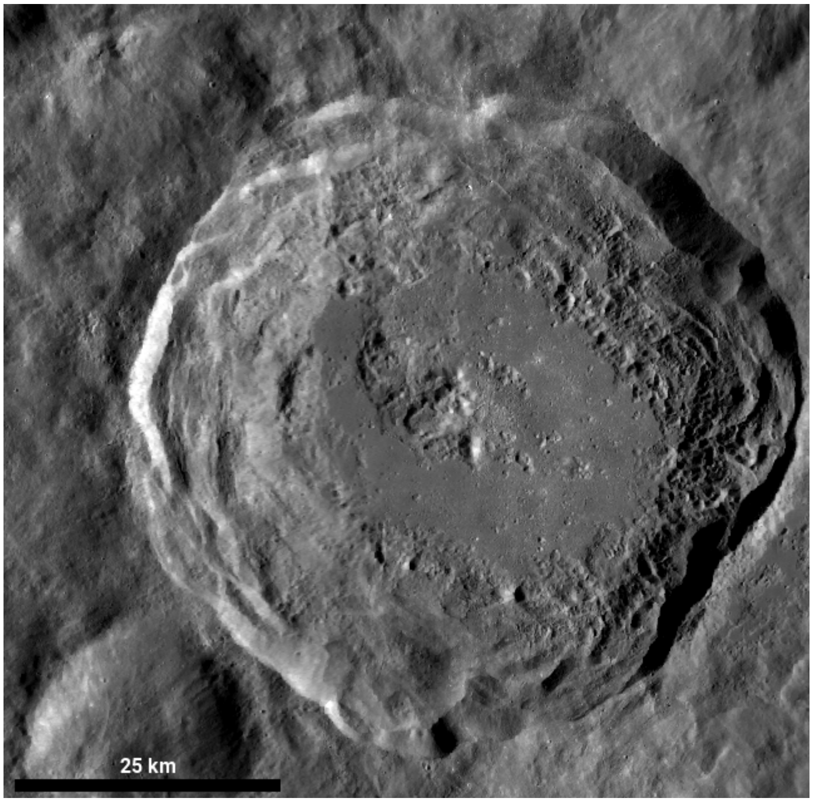

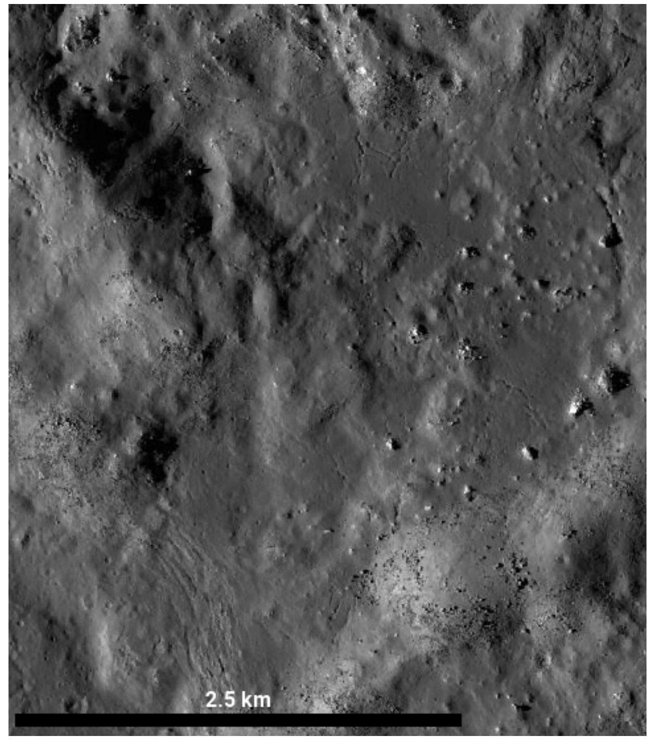

Figure 9: Ohm, 18.389°N, 246.189°E taken with LROC WAC. Impact melt-filled impact crater. Ohm is a crater with several terraces along its rim, as well as several deposits of smooth terrain around its central peak. The crater is covered in boulders and other ejecta. Figure 9a: 18.434°N, 246.045°E taken with LROC NAC. This was taken right on the edge of the central peak, and the bottom left is the base of the peak. Small linear features indicate where the flow pooled at the bottom of the peak, showing evidence of flow. Darker spots are clusters of boulders that the flow warped around. This terrain is smoother than the rest of the crater floor.

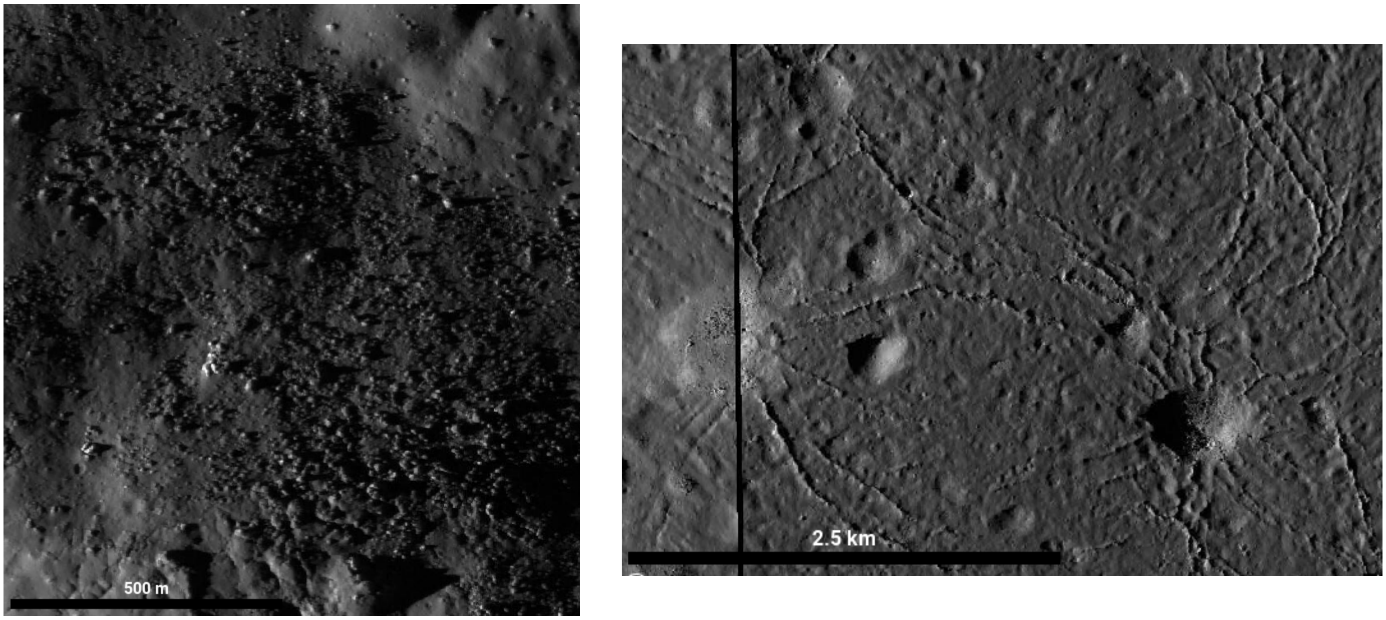

Figure 9b: 18.541°N, 246.051°E shown in LROC NAC images. An example of clusters of boulders on Ohm. These boulders formed during the impact that created Ohm and moved from higher elevations to settle in current locations. Figure 9c: 18.592°N, 246.427°E shown in LROC NAC images. Mounds of melt that solidified over preexisting terrain as well as boulders on top. Stress fractures formed around the mounds as the melt cooled and contracted.

Jackson (22.029°N, 196.643°E) measures at 71km in diameter and is the second impact melt-filled crater studied. It has a distinct terracing of its crater rim, as well as a ponded appearance (Fig. 10). There are numerous smooth pockets ponded on the crater rim. Other smooth deposits exist on the crater floor. These ponded deposits do not exceed 10km^2. The majority of the crater floor is covered in river-like terrain (Fig. 10a) with divets and rippling crust. These “ripple” features are <5km long and <1km wide, taking up approximately 80% of the crater floor. Mixed in with the ripples are multiple fractures. Neither the fractures nor the ripples follow a single pattern. Rather clusters of features may stretch in the same direction. Large mounds interrupt the features, but unlike the mounds on Ohm these are not surrounded by fractures (Fig. 10b). The flowing texture goes around the mounds and warps to their shape. The mounds' tops are covered in criss-crossing features and boulders. These mounds are the only other place where boulders exist in Jackson, aside from the central peak. Those boulders rest along the slope of the central peak, pooling towards the base of the peak. Jackson's central peak stretches upwards of 2000km above the crater floor. In the north rim of Jackson is a 7km solidified flow (Fig. 10c). The feature flows down the rim, going over a section of terraced rim and into the crater floor below. Right beneath the feature exists an example of small ponds of smooth terrain. Edges of the terraced rim near the feature also display a streaking appearance and pooling into the crater below. Jackson also has a massive ejecta output, extending 640km beyond the rim. Under the Clementine mineral ratio, Jackson is indistinguishable from the surrounding terrain, a mix of blue and red indicating high titanium in an ancient basin. Under the Fe/O ratio it is a bluer color for low iron.

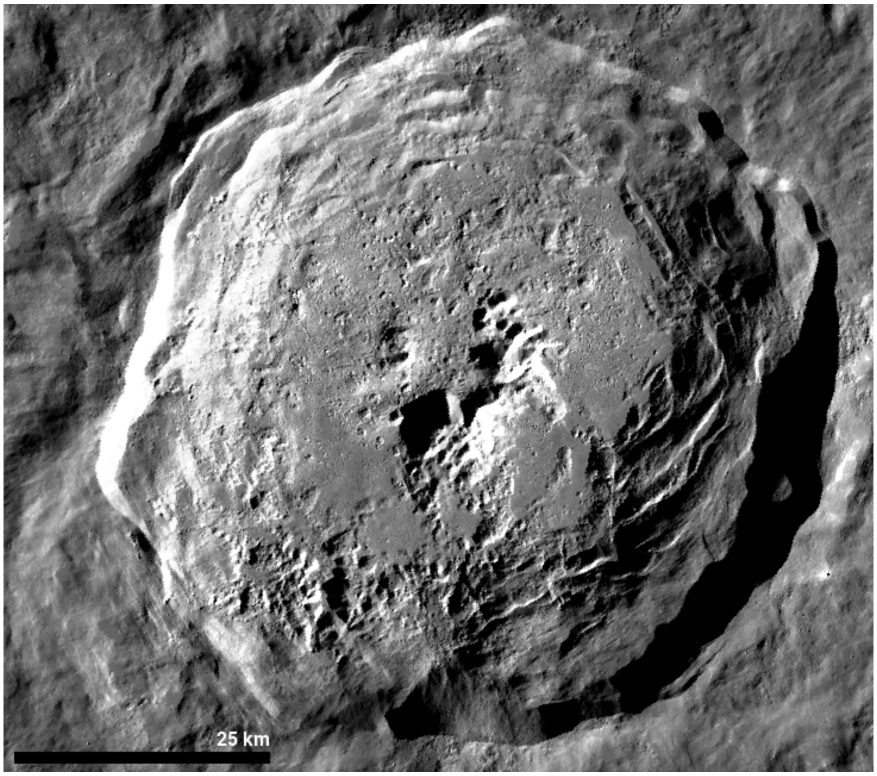

Figure 10: Jackson, 22.029°N, 196.643°E taken with LROC WAC. Impact melt-filed impact crater. Jackson appears ponded from a distance but the floor is rough and uneven, covered in small-scale features (<5km). Smooth deposits exist at lower elevations and <10km^2.

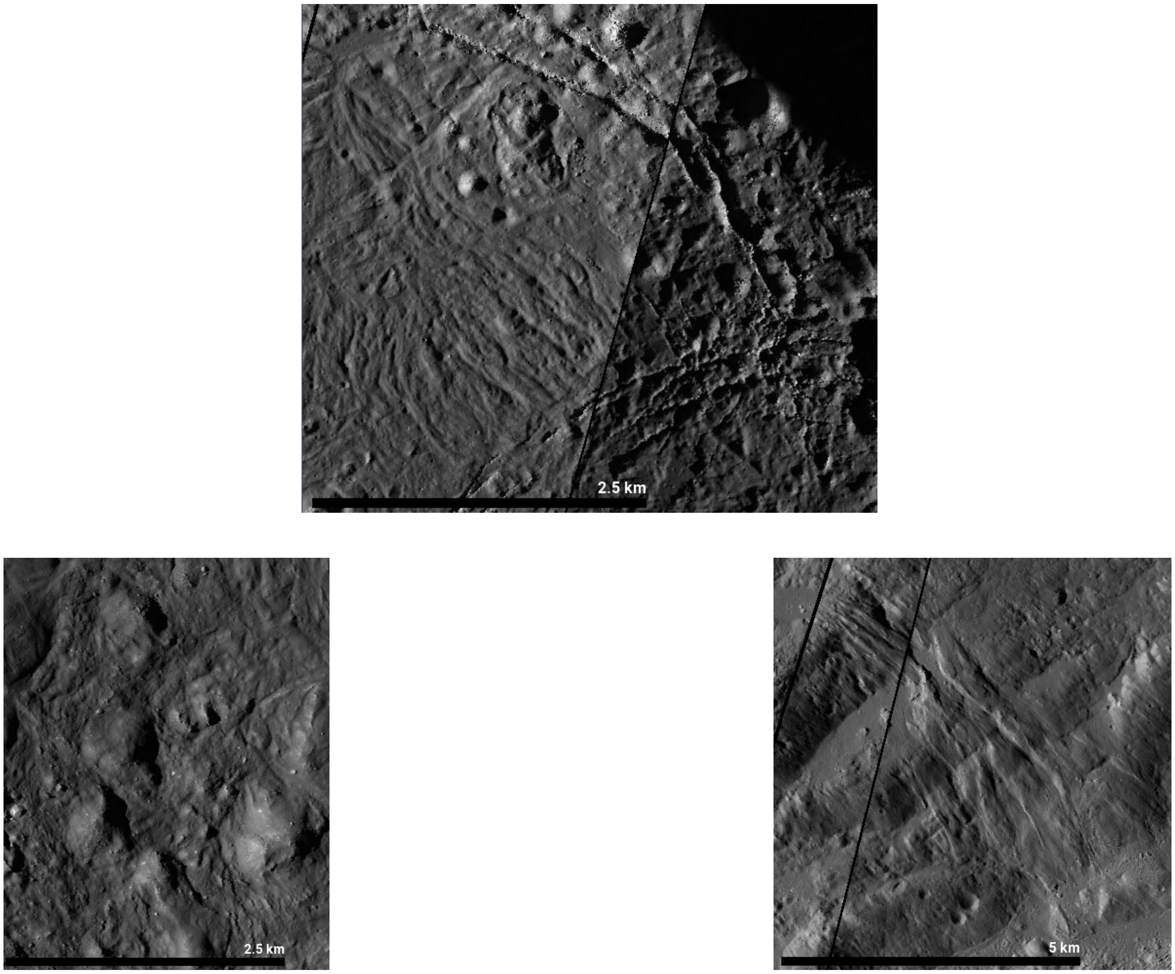

Figure 10a: 21.795°N, 196.21°E taken with LROC NAC. Small-scale features on Jackson (<5km) of indeterminate origin, though likely formed as the melt moved around in the crater floor. Several stress fractures seen to the right formed as melt cooled around pre existing terrain. Figure 10b: 22.123°N, 196.547°E taken with LROC NAC. Mounds that pre-existed the flow are covered by flow that moved around it and warped as it solidified. These are part of Jackson's small-scale features. Figure 10c: 22.61°N, 196.003°E taken with LROC NAC. Evidence of flow in the crater rim. Starts from the smooth deposit in the upper left and flows down into the crater floor. The flow solidified as it flowed and ponded at terraces. Places where it pooled are smoother than the rest of the floor.

Eratosthenes (14.703°N, 348.797°E) is an impact melt-filled crater measuring 60km in diameter (Fig. 11). The rim of Eratosthenes is remarkably well-preserved and terraced all the way around the crater. Eratosthenes' central peak is split into two peaks. One reaches approximately 2100km above the crater floor, while the other tops at about 700km above the floor (Fig. 11a). In between the peaks is a small valley, it is still a good 400km above the floor. The central peak area of Eratosthenes is connected to a rough terrain spanning from the peak to the northwest terraces. That terrace has partially collapsed. Small pockets of melt reside on terraces in the southeastern rim (Fig. 11b) approximately 8km long and 2km wide. The crater floor is covered in rounded mounds as well as secondary craters. The secondary craters are predominantly clustered in the south, and the mounds can be seen all over the crater floor. What separates the features on Eratosthenes from those in Ohm and Jackson is that all of these features are smoothed over. There are no linear features or fractures in solidified melt. The central peak is also rounded, with high albedo at the peak. That high albedo appears yellow under the Clementine mineral ratio, suggesting a low titanium content on its peak. A ring of light blue surrounds the crater under the mineral ratio as well, however, other than these two features, the crater appears to have the same mineral composition as its surroundings. Under the UVVIS/FeO abundance filter, Eratosthenes has the same chemical composition as its surroundings, which are a bright yellow and orange indicating high iron content. The peak and other spots on the crater floor are a bright blue, suggesting an overlay of ejecta low in iron.

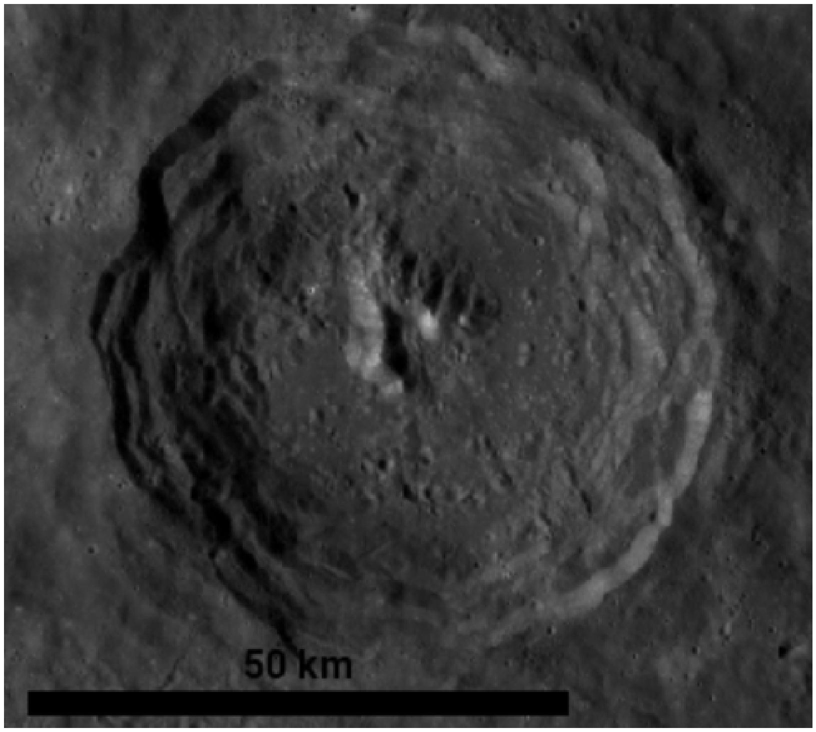

Figure 11: Eratosthenes, 14.703°N, 348.797°E taken with LROC WAC. Eratosthenes is an impact crater mostly covered by ejecta from younger craters nearby. The features of Eratosthenes are smoothed over and any small-scale features are covered by ejecta. What remains are the larger central peak and terraced rim.

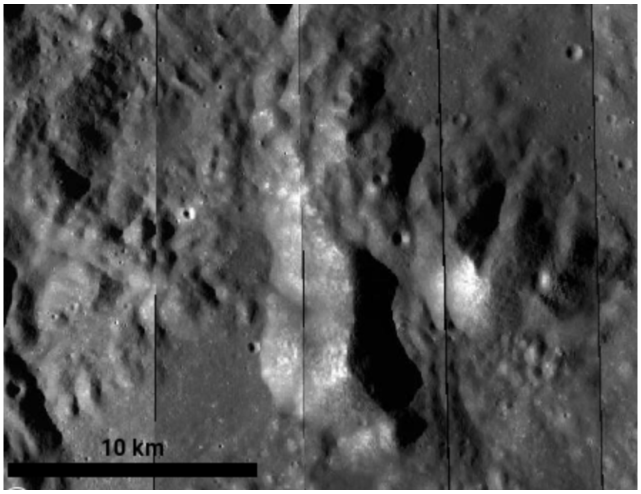

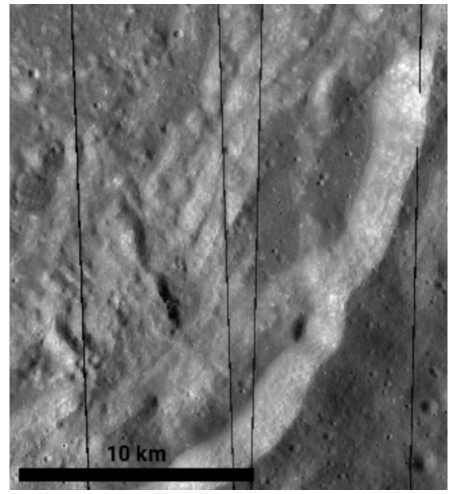

Figure 11a: 14.635°N, 348.559°E taken with LROC NAC. The central peak of Eratosthenes is split into several pieces as is the crater rim to the northwest. The crater floor is nonexistent in this portion of the crater, covered by the collapsed rim. Figure 11b: 9.059°N, 340.969°E taken with LROC NAC. Through the ejecta melt pools are still visible on the crater walls. The melt pools are no greater than 10km^2 and any sign of flow direction is obscured by the ejecta layer.

The final impact melt-filled crater studied is Copernicus (9.621°N, 339.921°E), located just southwest of Eratosthenes. It measures 93km in diameter, with rays extending upwards of 600km away from its center (Fig. 12). Copernicus is distinguishable by its significantly higher albedo than the surrounding Imbrium basin. The rim is intact all the way around the crater. The entire rim of the crater has a single terrace surrounding the crater, creating two distinct levels between the floor and rim. The major terrace has multiple melt pools all around the crater rim (Fig. 12a). Individual pools range from 3-10km long but never exceed 10km^2 overall. The central peak of

Copernicus is fractured into three peaks. The crater floor is covered with small-scale linear features (<3km) and mounds. Stress fractures congregate near the mounds and at the boundary between crater floor and terracing. The surface appears bumpy and heterogeneous in texture, similar to Jackson. Small mounds interrupt disjointed linear features with no discernible pattern to the floor's appearance (Fig. 12b). The largest mounds, as well as the central peak, are surrounded by and covered with clusters of boulders (Fig. 12c). The majority of the boulders can be found within the central peak, though a small number of boulders can be found scattered everywhere except the floor. Evidence of flow can be seen in the north portion of the crater, at the intersection between the terraces and crater floor (Fig. 12d). Under the Clementine mineral ratio, three quarters of the crater are a bright blue, indicating the youth (<1 Ga) of Copernicus. The northwest quadrant of the crater, and the rays surrounding the crater are bright red, significantly more red than the surrounding terrain. Under the UVVIS/FeO abundance filter. Copernicus lights up a practically neon blue in a sea of orange, suggesting a very low iron content compared to its surroundings.

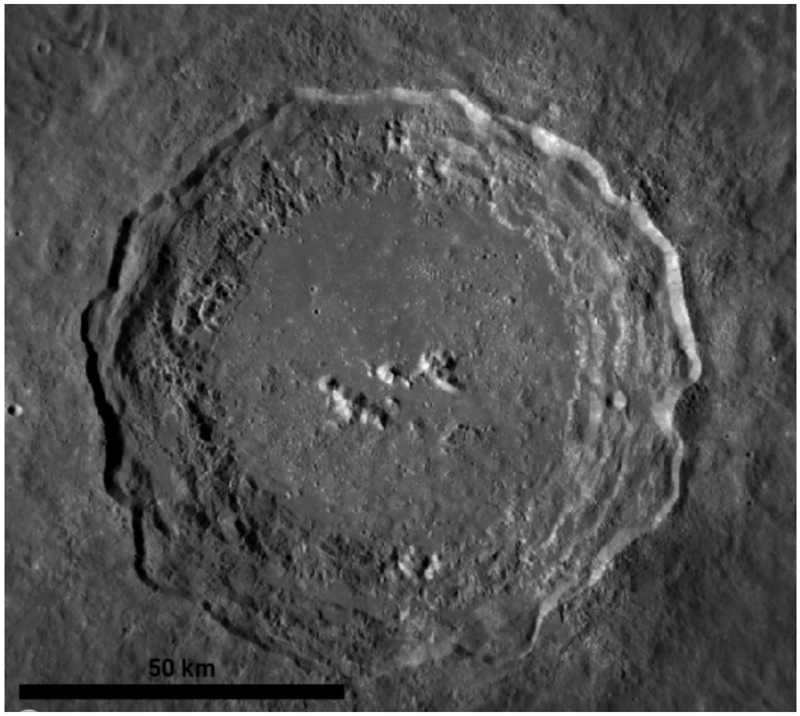

Figure 12: Copernicus, 9.621°N, 339.921°E taken with LROC WAC. Copernicus is one of the youngest impact melt-filled craters on the surface of the Moon. The rim is heavily terraced with ejecta spreading beyond the crater rim. The central peak is in several pieces and relatively small.

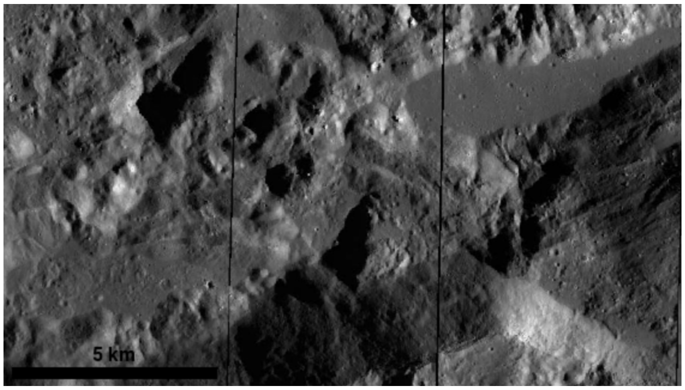

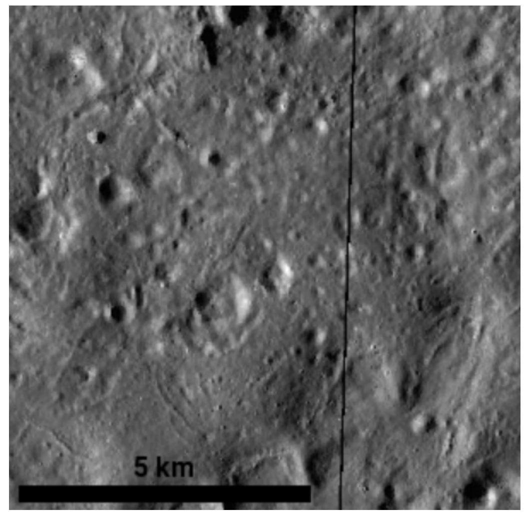

Figure 12a: 8.405°N, 340.134°E taken with LROC NAC. Examples of melt pools on the crater rim. Pools are no larger than $10km^2$ each. Some connect with one another by flowing down into the crater floor. The pools are separated by rough terrain from the crater floor. Figure 12b: 9.091°N, 340.138°E taken with LROC NAC. An example of Copernicus' crater floor. The terrain is rough with mounds scattered around. Stress fractures line the crater floor as well with no identifiable pattern. Figure 12c: 9.678°N, 340.239°E taken with LROC NAC. A section of the central peak system rises above the crater floor. The peak is lined with boulders that have settled on flat surfaces along the peak and onto the crater floor. A large collection of boulders have settled into the lower elevation areas of the central peak as well.

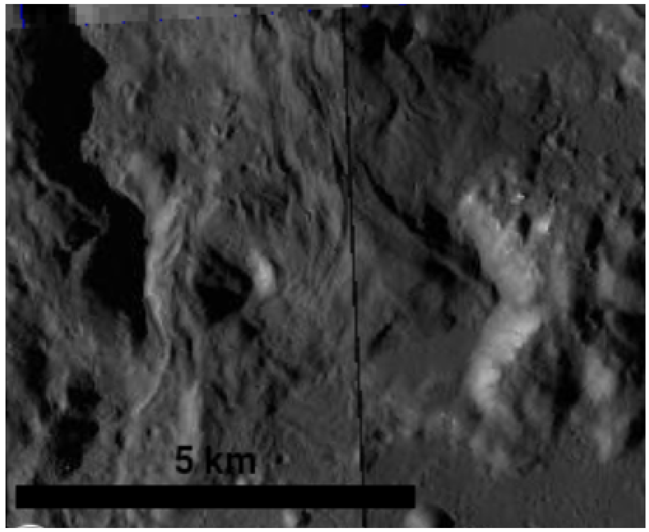

Figure 12d: 10.672°N, 339.765°E taken with LROC NAC. Evidence of flow on the rim of Copernicus. The melt flows from terraces into the crater floor where it pools enough to create a higher elevation than the nearby crater floor. Evidence of the flow branching off is visible with the features smoothed over.

5: Interpretations

This section provides interpretations of the craters in the same order as above and then with their groups.

One of Joliot's embayed craters is missing part of its rim, and is most likely underneath the fill. It was of a lower elevation than where the current crater floor is today (Fig. 5). This means that the embayed crater predates the fill, and was filled up at the same time as the rest of the floor. It is unclear if the flow filled the crater from inside to the brim like a glass of water, or if it flowed over where the rim is nonexistent. This is relevant, as there is only one other feature from pre existing topography that remains after volcanic material is emplaced: the central peak. Joliot's central peak has been transformed both at the peak and base. Over time, the peak erodes, and volcanic material rises to cover the base. In a similar fashion, the original central peak was filled in by volcanic material. The massive ridge formed as the mare cooled and contracted, causing local stress that pushed on the surface. Joliot's lighter albedo and obscured surface are due to the ejecta from nearby Giordano Bruno crater (35.9°N, 102.8°E), which has massive rays stretching hundreds of kilometers. The younger crater spewed massive amounts of ejecta across the surface, covering what would have been the smooth volcanic material of Joliot's crater floor. This and Joliot's secondary crater clusters are likely explained by its proximity to several other craters, including Lyapunov (26.429°N, 89.364°), Lomonosov (27.35°N, 98.279°E), and Edison (24.88°N, 99.268°E).

Most of the unique features of Tsiolkovskiy are due to its younger age compared to the other volcanically-filled impact craters. There has been less time for the initial impact features to degrade. This is most prominent in the rim, which is still distinct and terraced. Terracing occurs when the steep crater walls shift and fall due to gravity during the impact crater formation process. Tsiolkovskiy likely formed these terraces during crater formation. Another feature still prevalent in Tsiolkovskiy is the central peak. Over time regolith smooths over these features. There are no large craters near Tsiolkovskiy that could explain the small peaks in random places, or the secondary craters. While it is possible these are the remains of embayed craters, it is more likely a part of the central peak that is not visible in the other two craters, as they are not circular. Central peak formation is not a "clean" process, and it is possible that material was brought up from depth to form these features on the floor that later became partially buried by volcanic material. The origin for secondary craters is unclear, as secondary craters can occur hundreds of kilometers from the original crater.

The multiple superimposed craters support the old age of Jules Verne, as there has been more time for craters to impact into the basin. Either this section of the Moon’s surface was heavily altered previously, or the volcanic fill was low enough in volume to only partially obscure older craters. The small linear feature in and surrounding an embayed crater indicates a different layer of mare emplacement, and that the fill of this embayed crater flowed out of the crater floor and mixed with the rest of the melt. This implies that the volcanic flow was hampered by volume as opposed to surface area. The embayed crater filled up till the flow stopped, and only covered part of the peak.

The crater obscured by the magma must have been large enough that its central peak survived the series of flows.The massive scarp was caused by long-term interior cooling causing contraction and buckling of the lunar crust. It is likely that this scarp was a direct result of the cooling magma.

Archimedes' features are covered in a thin layer of ejecta from the nearby crater Aristillus (33.9°N, 1.2°E). Any features on the meter or smaller scale are obscured. The only prominent features visible over the layer of ejecta are secondary craters caused either by Archiemdes' initial formation or the ejection of debris from Aristillus. The latter is much more likely, given the craters have not been filled in with ejecta and are rather pronounced on the surface floor. Aristillus is not the only reason for Archimedes' smooth or missing features. Years of erosion and weathering would have made any small features disappear long before Aristillus covered the crater floor. As part of the Imbrium basin, it is important to note that Archimedes is younger than the initial Imbrium fill, approximately 3.8 Ga, though not by much. The chemical composition and albedo of Archimedes is the same as the basin. The source of the Imbrium basin fill is likely the same as in Archimedes, meaning the crater must be only slightly younger than the basin. The northwestern linear features suggest at least two flows of volcanic melt at different times. If there was a central peak, it was either obscured during crater filling or eroded away over the eons. While the walls are intact, the modest height and lack of distinct terracing support the age argument.

The most notable feature that all four craters share is a lower albedo in comparison to the highlands terrain. That lower albedo is the filled in crater floor, and is predominantly smooth with little elevation change. Higher albedo surrounds the fill, forming the crater walls and rim. These rims are not entirely intact. A fully intact rim is part of a complex crater, when the rim is distinct and unobstructed. Both Joliot and Jules Verne show superimposed craters obscuring part of the rim. Three craters also appear yellow on the Clementine Mineral Ratio, indicating the same titanium ratio, as if they all had the relatively same composition. The one distinction is Archimedes, which shows the same composition as the surrounding Imbrium basin. Joliot and Jules Verne have observable embayed craters, while Tsiolkovskiy has possible remnants, indicating a preexisting terrain was destroyed during flow and is now obscured by material. Each crater displays optical maturity. This refers to a layer of iron covering older lunar surfaces due to solar radiation and <1 mm meteorite bombardments. It is important to note that these features are all a consequence of or evidence of old age; as most volcanic activity occurred between 3.9-3.1 billion years ago, with the youngest bouts of volcanism estimated at 1 billion years, all of these craters should date to that time (Braden et al., 2011). Ignoring superimposed craters, the volcanic material itself manifests in a smooth surface that covers any preexisting features, leaving only a few large linear features. These features formed either when the volcanic fill cooled, or when multiple flows filled in the crater at different intervals. This is in direct contrast to the tiny but numerous linear features in impact melt-filled impact melt-filled craters. Regolith generation occurs over time through iron meteorite bombardment. All surfaces on the Moon have a layer of regolith, where the older surfaces have thicker layers. The regolith layer softens and erases small-scale features on the lunar surface. What this means is that the fill in Tsiolkovskiy and other volcanically-filled impact craters likely had small scale features such as cooling cracks and flow features but that billions of years of regolith development basically erased evidence of these features.

The mounds on Ohm likely originate from before the impact material was emplaced. When melt flowed over the original topography, it warped around the surface. As it cooled, the material broke and fractured around the original material. Most stress fractures are in fact a reflection of or caused by the surface before and after melt emplacement. As the melt cooled, it was confined to the shape it was contained in, as did the stress it endured, so fractures propagated along the shape. Ohm's boulders, on the other hand, are either formed during the initial impact and ejected or post crater modification from rock settling (Bart and Melosh, 2010). They may roll before finding stable positions, such as the boulders surrounding the central peak. Flow on the central peak shows the direction in which the melt moved, piling up at the base of the peak as it cooled.

Jackson's small ponds of smooth melt deposits likely formed as the final resting spots of impact melt that originated at higher elevations. The most obvious example of this is fig. 10c, where flow solidified as it ran down the crater wall and into terraces of lower elevations. The deposits of smooth terrain occur at the lowest elevations of Jackson, for example at the floor of the central peak, therefore suggesting that any melt that flowed down the peak ponded at its base. In regards to the rest of the floor, however, its origin is unclear. The impact crater creation process is highly energetic, resulting in large-scale slumping and melting of material in a very brief period of time (Dhingra et al., 2017). The melt material sloshed around as it cooled, still carrying the energy of the impact, resulting in the unique patterns across Jackson's surface. This is likely also the explanation for the mounds and their unique surrounding topography. As the melt flowed, it moved around the boulders that had been emplaced during impact. There was not enough energy to move the boulders themselves, only enough to move the remaining still-liquid melt. This theory would still require a high-energy initial impact, which would further explain the unique appearance of Jackson under the Clementine Mineral Ratio. The bright blue rays extending several hundred kilometers suggests a high velocity impact that sent ejecta flying. That kind of energy would also result in the violent movement of melt required.

Eratosthenes has features in common with both volcanic and impact melt-filled craters, due in large part to its age. At over 3 Ga (Taylor 1982) it is considerably older than the other impact craters. Eratosthenes has a high iron content in and surrounding the crater, similar to the basaltic mare. However, this is not due to a basaltic fill, but instead the result of space weathering (ie optical maturity). Optical maturity comes with age, which is why the ancient mare fills are always high in iron. Any linear features on the crater floor have faded away over time. That includes boulders or stress fractures, such as those seen in the other impact melt-filled craters. Erosion may have also caused the collapse of the central rim, forming the dual nature seen. This seems unlikely, because the valley between central peaks matches the appearance of the crater floor nearby. It is heavily eroded, signaling the valley to be the same age as the crater floor. Instead, the dual peaks are a consequence of initial formation. The two peaks were initially one but collapsed while solidifying, as also happened in the northwest terraces. Interestingly, Eratosthenes’ crater rim is intact and prominent, which could have been interpreted to be a sign of a younger crater. Terraced rims are not a sign of age (although they can slump and decrease in elevation over time), but rather, are a feature unique to impact craters that volcanically-filled craters lose when the crater fills up. If the volume is high enough, entire terrace levels may be obscured. Meanwhile, impact melt-filled craters never fill the crater beyond the floor, and thus without outside interference the terraces may remain for a long time.

Copernicus is one of the youngest craters on the Moon (Eberhardt, 1982), and thus serves as a primary example for what features are unique to impact melt-filled craters. The separation of the central peak further suggests that central peak collapse occurs during initial crater formation. As the initial crater collapses, uplifting at the floor creates central peaks. The process lifts up material beneath the pre-impact surface, revealing the composition of the Moon’s mantle. The process of uplifting requires enormous amounts of energy, and thus not all of the mantle beneath the crater may rise up. The individual peaks may represent an uneven crustal thickness prior to impact. The boulders on top of and surrounding the central peak are likely remnants from the initial impact. As the crater settled, boulders rolled downward and settled in lower portions of the central peak, as well as on the crater floor. Undisturbed central peaks may have a different albedo or chemical composition than the surrounding crater floor, as is the case with Copernicus. The distinct difference in mineral composition seen in the northwest quadrant of Copernicus suggests an ancient basin that would not be possible unless it is the preexisting material displaced by Copernicus.

Instead of the distinct color difference prevalent in volcanically-filled impact craters, impact melt-filled craters appear the same albedo as the surrounding terrain. Under the Clementine UVVIS ratio, for example, Jackson appears the same shades of blue, meaning low-iron, as the surrounding terrain. This is in direct contrast to the intense orange and yellows of volcanically-filled impact craters such as Tsiolkovskiy. While older craters such as Eratosthenes can appear high in iron, the importance is that the chemical composition of impact filled craters be of the surrounding terrain. Volcanically-filled impact crater floors are of a different composition from the surrounding terrain, a magnesium and iron-rich basalt, due to the composition of the magma beneath the surface. Impact melt-filled craters display a rim of bluer material than the surrounding terrain, indicating a younger age. The crater floor is typically a mix of impactor and preexisting material, however central peaks can exhibit more mare-like ancient compositions. A simplified chart illustrating the characteristics for each crater and observed features/feature types is presented in Table 1.

	Archimedes	Copernicus	Eratosthenes	Jackson	Joliot	Jules Verne	Ohm	Tsiolkovsky
Low relative albedo	y	n	n	n	y	y	n	y
Ponded	n	y	y	y	n	n	y	n
embayed craters	n	n	n	n	y	y	n	n
visible ejecta	n	y	y	y	n	n	y	n
Iron content	high	low	medium-high	low	high	high	low	high
200m mineral ratio	red and green	blue and red	blue and yellow	blue and red	blue, red, green	yellow and green	blue	yellow, green, blue
central peak	n	y	y	y	y	y	y	y
superposed craters	n	n	n	n	y	y	n	n
Intact rim on all sides	n	y	y	y	n	n	y	y
terraced rim	y	y	y	y	n	n	y	y
smooth regolith	y	n	y	n	y	y	n	y
boulders	n	y	n	y	n	n	y	n
mounds	n	y	y	y	n	n	y	n
cooling fractures	n	y	n	y	n	y	y	n
secondary impact craters	y	n	y	n	y	y	n	y
superposed ejecta	y	n	y	n	y	y	n	n
visible flow	n	y	y	y	n	y	y	n
wrinkle ridge	n	n	n	n	y	y	n	n
rough crater floor	n	y	n	y	n	n	y	n
melt pool on walls	n	y	y	y	n	n	y	n

large ($>10km^2$) scale linear features	y	n	n	n	y	y	n	y
small scale ($<10km^2$) linear features	n	y	n	y	n	n	y	n

Table 1: Table of distinct features and which craters harbor said feature. The 200m mineral ratio is too complicated for a quick summary, so the colors have been listed (what they mean can be found in methods). The most notable are iron content, terraced rim, boulders, melt pool on walls, secondary impact craters, visible flow, and the scale linear features.

The chart demonstrates the characteristics that are shared between the types of flow, as which features are more synonymous with age. Embayed craters, for example, are only found in volcanically-filled craters because of the mechanism in which they fill. They are not required to determine a volcanically-filled crater. But if an embayed crater is present, then the crater is volcanically-filled. A similar property is the presence of small-scale features. Older impact craters like Eratosthenes no longer have small linear features. Younger impact craters have not eroded or weathered enough for the features created by impact to have faded away. Therefore, mounds, boulders, and other evidence for impact events are only found in craters with impact melt.

All craters, both volcanic and impact-filled, start off as impact melt-filled craters. As such, some features that are created during crater formation can exist in both types of craters. Terraced rims are caused by the initial impact, however they erode and slump over time. An older crater is less likely to have intact rims, and volcanic craters are typically older, but the presence or absence of terraced rims alone cannot determine the fill type.

By examining the two extreme ends of lunar crater ages, I am able to see which features are retained over the eons and which are a function of age. Aside from the color similarities, All four craters had the same interesting morphology in common. The craters had distinct, intact rims with terracing. The intact and prominent wall allows for a distinct boundary between crater and surrounding terrain. All of the craters had a central peak still intact, and in Jackson extends upwards of 2000km above the crater floor. While central peaks exist in volcanically-filled impact craters, the fill and regolith layer has covered up the lower original crater floor, and therefore the peak appears shorter. Another feature that appears due to the same principle is the embayed craters, which none of the impact melt-filled craters have. Any preexisting craters would have been obliterated in the initial impact. There are also no superposed craters. As younger, fresher impacts, there has not been any time for new craters to impact and shape the crater floor. The presence of small-scale linear features is a function of age. Larger structures remain over the eons, but meter-scale linear features, boulders, and mounds erode with age. Of the impact craters, Eratosthenes was the only one without significant defacing of the crater floor, and even then evidence of prior formations remain in rounded mounds.

6: Conclusions

Several characteristics appear in both volcanically and impact melt-filled impact craters, though there are clear differences and patterns that arise in this format. Craters with the same composition retain a similar pattern under the maps. Volcanically filled impact craters are high in iron and low in titanium, and appear older and darker than the surrounding terrain. They are dotted with superposed and embayed craters, as well as having a smooth regolith. Finally, the volcanically-filled impact craters all have a few large-scale (>10km^2) linear features, such as scarps and wrinkle ridges. The impact melt-filled impact craters are the opposite. They appear the same albedo and composition of their surroundings, in part due to their large ejecta fields. The younger craters are low in iron, indicating that they are not composed of the same basaltic flow. Any iron seen in older impact craters is of differing composition and due to space weathering. While they appear ponded at a distance, the impact melt-filled impact craters contain several small scale (<10km^2) features that extend across the crater floor. Their walls are terraced, with smooth ponds atop the terraces. Direction of flow is prevalent, indicating a slow-moving mixture.

Only eight craters were examined in this study, far too small for definitive generalization. Furthermore, all the craters examined in this study were larger than 60km in diameter. It is entirely possible that certain features only occur in a certain size range. Some craters may be too small for superposed or embayed craters, for example. It may also be the case the other way around; that certain features only occur in craters smaller than a certain size. Further restrictions are due to the age of craters in question. The Moon is geologically inactive. There are no young mare deposits to observe and compare to. While there are impact craters of the same age as volcanically-filled craters, they are few and far between, as older craters are wiped out by new ones. Further study of craters of various sizes is needed for a definitive answer. The literature seems to have a similar problem to my study, in that small pockets of the Moon’s surface are viewed in each study. Over several papers, a broader view of the Moon’s surface may be reached, but no one individual research paper has authority in this regard.

7: Bibliography

Antonenko, Irene, et al. “Criteria for the Detection of Lunar Cryptomaria.” *Earth, Moon, and Planets*, vol. 69, no. 2, 2, Jan. 1995, pp. 141–72. *Springer Link*, https://doi.org/10.1007/BF00613096.

Ashley, J. W., et al. “Geology of the King Crater Region: New Insights into Impact Melt Dynamics on the Moon.” *Journal of Geophysical Research: Planets*, vol. 117, no. E12, E12, 2012. *Wiley Online Library*, https://doi.org/10.1029/2011JE003990.

Bandfield, Joshua L., et al. “Lunar Surface Rock Abundance and Regolith Fines Temperatures Derived from LRO Diviner Radiometer Data.” *Journal of Geophysical Research: Planets*, vol. 116, no. E12, E12, 2011. *Wiley Online Library*, https://doi.org/10.1029/2011JE003866.

Bell, Jeffrey F., and B. Ray Hawke. “Lunar Dark-Haloed Impact Craters: Origin and Implications for Early Mare Volcanism.” *Journal of Geophysical Research: Solid Earth*, vol. 89, no. B8, B8, 1984, pp. 6899–910. *Wiley Online Library*, https://doi.org/10.1029/JB089iB08p06899.

Belton, M. J. S., et al. “Galileo Multispectral Imaging of the North Polar and Eastern Limb Regions of the Moon.” *Science*, vol. 264, no. 5162, 5162, May 1994, pp. 1112–15. *science.org (Atypon)*, https://doi.org/10.1126/science.264.5162.1112.

Binder, Alan B. “Lunar Prospector: Overview.” *Science*, vol. 281, no. 5382, Sept. 1998, pp. 1475–76. *DOI.org (Crossref)*, https://doi.org/10.1126/science.281.5382.1475.

Boyd, A. K., et al. *LROC WAC 100 Meter Scale Photometrically Normalized Map of the Moon*. Dec. 2013, pp. P13B-1744.

Bray, V. J., et al. “New Insight into Lunar Impact Melt Mobility from the LRO Camera.” *Geophysical Research Letters*, vol. 37, no. 21, 21, 2010. *Wiley Online Library*, https://doi.org/10.1029/2010GL044666.

Bray, Veronica J., et al. “Lobate Impact Melt Flows within the Extended Ejecta Blanket of Pierazzo Crater.” *Icarus*, vol. 301, Feb. 2018, pp. 26–36. *ScienceDirect*, https://doi.org/10.1016/j.icarus.2017.10.002.

Campbell, Bruce A., et al. “Earth-Based 12.6-Cm Wavelength Radar Mapping of the Moon: New Views of Impact Melt Distribution and Mare Physical Properties.” *Icarus*, vol. 208, no. 2, 2, Aug. 2010, pp. 565–73. *ScienceDirect*, https://doi.org/10.1016/j.icarus.2010.03.011.

Carter, Lynn M., et al. “Initial Observations of Lunar Impact Melts and Ejecta Flows with the Mini-RF Radar.” *Journal of Geophysical Research: Planets*, vol. 117, no. E12, E12, 2012. *Wiley Online Library*, https://doi.org/10.1029/2011JE003911.

Characterization of Space Weathering from Lunar Reconnaissance Orbiter Camera Ultraviolet Observations of the Moon - Denevi - 2014 - Journal of Geophysical Research: Planets - Wiley Online Library.

https://agupubs.onlinelibrary.wiley.com/doi/full/10.1002/2013JE004527. Accessed 30 Jan. 2022.

Christensen, P. R., et al. *JMARS - A Planetary GIS*. Dec. 2009, pp. IN22A-06.

Cintala, Mark J., and Richard a. F. Grieve. “Scaling Impact Melting and Crater Dimensions: Implications for the Lunar Cratering Record.” *Meteoritics & Planetary Science*, vol. 33, no. 4, 4, 1998, pp. 889–912. *Wiley Online Library*, https://doi.org/10.1111/j.1945-5100.1998.tb01695.x.

Comparison of the Crater Morphology-Size Relationship for Mars, Moon, and Mercury - ScienceDirect. 7 Dec. 2021, https://www.sciencedirect.com/science/article/pii/0019103576901275?via%3Dihub.

Courses in Astrophotography. http://www.damianpeach.com/lunar12.htm. Accessed 30 Jan. 2022.

Daubar, Ingrid J., et al. “The Morphology of Small Fresh Craters on Mars and the Moon.” *Journal of Geophysical Research: Planets*, vol. 119, no. 12, 12, 2014, pp. 2620–39. *Wiley Online Library*, https://doi.org/10.1002/2014JE004671.

Denevi, Brett W., et al. “Physical Constraints on Impact Melt Properties from Lunar Reconnaissance Orbiter Camera Images.” *Icarus*, vol. 219, no. 2, 2, June 2012, pp. 665–75. *ScienceDirect*, https://doi.org/10.1016/j.icarus.2012.03.020.

Dhingra, Deepak, et al. “Geological Mapping of Impact Melt Deposits at Lunar Complex Craters Jackson and Tycho: Morphologic and Topographic Diversity and Relation to the Cratering Process.” *Icarus*, vol. 283, Feb. 2017, pp. 268–81. *ScienceDirect*, https://doi.org/10.1016/j.icarus.2016.05.004.

French, Renee A., et al. “Small-Scale Lunar Graben: Distribution, Dimensions, and Formation Processes.” *Icarus*, vol. 252, May 2015, pp. 95–106. *ScienceDirect*, https://doi.org/10.1016/j.icarus.2014.12.031.

Geological Mapping of Impact Melt Deposits at Lunar Complex Craters Jackson and Tycho: Morphologic and Topographic Diversity and Relation to the Cratering Process - ScienceDirect. https://www.sciencedirect.com/science/article/pii/S0019103516301403?via%3Dihub. Accessed 30 Dec. 2021.

Geology and Stratigraphy of King Crater, Lunar Farside - ScienceDirect. 7 Dec. 2021, https://www.sciencedirect.com/science/article/pii/S0019103502000635?via%3Dihub.

Gillis, Jeffrey J., et al. “Lunar Surface Geochemistry: Global Concentrations of Th, K, and FeO as Derived from Lunar Prospector and Clementine Data.” *Geochimica et Cosmochimica Acta*, vol. 68, no. 18, Sept. 2004, pp. 3791–805. *ScienceDirect*, https://doi.org/10.1016/j.gca.2004.03.024.

Giordano Bruno: Small Crater Populations—Implications for Self-Secondary Cratering - ScienceDirect. 7 Dec. 2021, https://www.sciencedirect.com/science/article/pii/S0019103518305967.

Greeley, Ronald, et al. “Galileo Imaging Observations of Lunar Maria and Related Deposits.” *Journal of Geophysical Research: Planets*, vol. 98, no. E9, E9, 1993, pp. 17183–205. *Wiley Online Library*, https://doi.org/10.1029/93JE01000.

Guo, Dijun, Wenzhe Fa, Xiaojia Zeng, et al. “Geochemistry of the Von Kármán Crater Floor and Thickness of the Non-Mare Ejecta over the Chang’e-4 Landing Area.” *Icarus*, vol. 359, May 2021, p. 114327. *ScienceDirect*, https://doi.org/10.1016/j.icarus.2021.114327.

Guo, Dijun, Wenzhe Fa, Bo Wu, et al. “Millimeter- to Decimeter-Scale Surface Roughness of the Moon at the Chang’e-4 Exploration Region.” *Geophysical Research Letters*, vol. 48, no. 19, 19, 2021, p. e2021GL094931. *Wiley Online Library*, https://doi.org/10.1029/2021GL094931.

Hawke, B. R., et al. *The Composition and Origin of Selected Lunar Crater Rays*. 1999, p. 22. *NASA ADS*, https://ui.adsabs.harvard.edu/abs/1999nvm..conf...22H.

Head III, James W. “Lunar Volcanism in Space and Time.” *Reviews of Geophysics*, vol. 14, no. 2, 2, 1976, pp. 265–300. *Wiley Online Library*, https://doi.org/10.1029/RG014i002p00265.

Head, James W., et al. “Lunar Impact Basins: New Data for the Western Limb and Far Side (Orientale and South Pole-Aitken Basins) from the First Galileo Flyby.” *Journal of Geophysical Research: Planets*, vol. 98, no. E9, E9, 1993, pp. 17149–81. *Wiley Online Library*, https://doi.org/10.1029/93JE01278.

Head, James W., and Lionel Wilson. “Lunar Mare Volcanism: Stratigraphy, Eruption Conditions, and the Evolution of Secondary Crusts.” *Geochimica et Cosmochimica Acta*, vol. 56, no. 6, 6, June 1992, pp. 2155–75. *ScienceDirect*, https://doi.org/10.1016/0016-7037(92)90183-J.

Heather, David J., and Sarah K. Dunkin. “Geology and Stratigraphy of King Crater, Lunar Farside.” *Icarus*, vol. 163, no. 2, 2, June 2003, pp. 307–29. *ScienceDirect*, https://doi.org/10.1016/S0019-1035(02)00063-5.

Hiesinger, H., et al. “Ages and Stratigraphy of Mare Basalts in Oceanus Procellarum, Mare Nubium, Mare Cognitum, and Mare Insularum.” *Journal of Geophysical Research: Planets*, vol. 108, no. E7, E7, 2003. *Wiley Online Library*, https://doi.org/10.1029/2002JE001985.

Hiesinger, Harald, et al. “Ages of Mare Basalts on the Lunar Nearside.” *Journal of Geophysical Research: Planets*, vol. 105, no. E12, E12, 2000, pp. 29239–75. *Wiley Online Library*, https://doi.org/10.1029/2000JE001244.

Hiesinger, Harald, and James W. Head III. “New Views of Lunar Geoscience: An Introduction and Overview.” *Reviews in Mineralogy and Geochemistry*, vol. 60, no. 1, 1, Jan. 2006, pp. 1–81. *Silverchair*, https://doi.org/10.2138/rmg.2006.60.1.

Holsapple, Keith A. “Impact Cratering; A Geological Process.” *Science*, vol. 245, no. 4923, 4923, Sept. 1989, pp. 1261–63.

Howard, Ka, and Hg Wilshire. “Flows of Impact Melt at Lunar Craters.” *Journal of Research of the Us Geological Survey*, vol. 3, no. 2, 1975, pp. 237–51.

Investigation of the Source Region of the Lunar-Meteorite Group with the Remote Sensing Datasets: Implication for the Origin of Mare Volcanism in Mare Imbrium - ScienceDirect. 7 Dec. 2021, https://www.sciencedirect.com/science/article/pii/S0019103521003468?via%3Dihub.

Jaumann, R., et al. “Geology, Geochemistry, and Geophysics of the Moon: Status of Current Understanding.” *Planetary and Space Science*, vol. 74, no. 1, 1, Dec. 2012, pp. 15–41. *ScienceDirect*, https://doi.org/10.1016/j.pss.2012.08.019.

Kereszturi, A., and V. Steinmann. “Terra-Mare Comparison of Small Young Craters on the Moon.” *Icarus*, vol. 322, Apr. 2019, pp. 54–68. *ScienceDirect*, https://doi.org/10.1016/j.icarus.2018.12.039.

Khan, A., et al. “Geophysical Evidence for Melt in the Deep Lunar Interior and Implications for Lunar Evolution.” *Journal of Geophysical Research: Planets*, vol. 119, no. 10, 2014, pp. 2197–221. *Wiley Online Library*, https://doi.org/10.1002/2014JE004661.

Koeberl, Christian. *CRATERS ON THE MOON FROM GALILEO TO WEGENER: A SHORT HISTORY OF THE IMPACT HYPOTHESIS, AND IMPLICATIONS FOR THE STUDY OF TERRESTRIAL IMPACT CRATERS*. p. 16.

Kreslavsky, M. A., and J. W. Head. “New Observational Evidence of Global Seismic Effects of Basin-Forming Impacts on the Moon from Lunar Reconnaissance Orbiter Lunar Orbiter Laser Altimeter Data.” *Journal of Geophysical Research: Planets*, vol. 117, no. E12, E12, 2012. *Wiley Online Library*, https://doi.org/10.1029/2011JE003975.

Kreslavsky, Mikhail A., et al. “Lunar Topographic Roughness Maps from Lunar Orbiter Laser Altimeter (LOLA) Data: Scale Dependence and Correlation with Geologic Features and Units.” *Icarus*, vol. 226, no. 1, 1, Sept. 2013, pp. 52–66. *ScienceDirect*, https://doi.org/10.1016/j.icarus.2013.04.027.

Krüger, T., et al. “Geomorphologic Mapping of the Lunar Crater Tycho and Its Impact Melt Deposits.” *Icarus*, vol. 273, July 2016, pp. 164–81. *ScienceDirect*, https://doi.org/10.1016/j.icarus.2016.02.018.

Laneuville, M., et al. “Asymmetric Thermal Evolution of the Moon.” *Journal of Geophysical Research: Planets*, vol. 118, no. 7, 2013, pp. 1435–52. *Wiley Online Library*, https://doi.org/10.1002/jgre.20103.

Lawrence, D. J., et al. “Thorium Abundances on the Lunar Surface.” *Journal of Geophysical Research: Planets*, vol. 105, no. E8, 2000, pp. 20307–31. *Wiley Online Library*, https://doi.org/10.1029/1999JE001177.

Lev, Einat, et al. “Emplacement Conditions of Lunar Impact Melt Flows.” *Icarus*, vol. 369, Nov. 2021, p. 114578. *ScienceDirect*, https://doi.org/10.1016/j.icarus.2021.114578.

Li, Yuan, and Bo Wu. “Analysis of Rock Abundance on Lunar Surface From Orbital and Descent Images Using Automatic Rock Detection.” *Journal of Geophysical Research: Planets*, vol. 123, no. 5, 2018, pp. 1061–88. *Wiley Online Library*, https://doi.org/10.1029/2017JE005496.

Lucey, Paul, et al. “Understanding the Lunar Surface and Space-Moon Interactions.” *Reviews in Mineralogy and Geochemistry*, vol. 60, no. 1, Jan. 2006, pp. 83–219. *Silverchair*, https://doi.org/10.2138/rmg.2006.60.2.

Lucey, Paul G., et al. “Lunar Iron and Titanium Abundance Algorithms Based on Final Processing of Clementine Ultraviolet-Visible Images.” *Journal of Geophysical Research: Planets*, vol. 105, no. E8, E8, 2000, pp. 20297–305. *Wiley Online Library*, https://doi.org/10.1029/1999JE001117.

Lunar Global Shape and Polar Topography Derived from Kaguya-LALT Laser Altimetry. 7 Dec. 2021, https://www.science.org/doi/10.1126/science.1164146.

Lunar Impact Basins Revealed by Gravity Recovery and Interior Laboratory Measurements. 7 Dec. 2021, https://www.science.org/doi/10.1126/sciadv.1500852.

Melosh, H. J., and B. A. Ivanov. “Impact Crater Collapse.” *Annual Review of Earth and Planetary Sciences*, vol. 27, no. 1, 1, 1999, pp. 385–415. *Annual Reviews*, https://doi.org/10.1146/annurev.earth.27.1.385.

Meter‐Scale Topographic Roughness of the Moon: The Effect of Small Impact Craters - Cai - 2020 - Journal of Geophysical Research: Planets - Wiley Online Library. 7 Dec. 2021, https://agupubs.onlinelibrary.wiley.com/doi/full/10.1029/2020JE006429.

Moon: Origin and Evolution of Multi-Ring Basins. p. 76.

Nagaoka, Hiroshi, et al. “Investigation of the Source Region of the Lunar-Meteorite Group with the Remote Sensing Datasets: Implication for the Origin of Mare Volcanism in Mare Imbrium.” *Icarus*, vol. 370, Dec. 2021, p. 114690. *ScienceDirect*, https://doi.org/10.1016/j.icarus.2021.114690.

NASA - Archimedes - Mare Flooded Crater! Brian Dunbar, https://www.nasa.gov/mission_pages/LRO/multimedia/lroimages/lroc-20110302-archimedes.html. Accessed 9 Apr. 2022.

Neish, C. D., et al. “Global Distribution of Lunar Impact Melt Flows.” *Icarus*, vol. 239, Sept. 2014, pp. 105–17. *ScienceDirect*, https://doi.org/10.1016/j.icarus.2014.05.049.

O'Rourke, Joseph G., et al. "Venus: Interpreting the Spatial Distribution of Volcanically Modified Craters." *Geophysical Research Letters*, vol. 41, no. 23, 2014, pp. 8252–60. *Wiley Online Library*, https://doi.org/10.1002/2014GL062121.

Osinski, G. R., et al. "The Effect of Target Lithology on the Products of Impact Melting." *Meteoritics & Planetary Science*, vol. 43, no. 12, 12, 2008, pp. 1939–54. *Wiley Online Library*, https://doi.org/10.1111/j.1945-5100.2008.tb00654.x.

Petro, Noah E., and Carlé M. Pieters. "Surviving the Heavy Bombardment: Ancient Material at the Surface of South Pole-Aitken Basin." *Journal of Geophysical Research: Planets*, vol. 109, no. E6, E6, 2004. *Wiley Online Library*, https://doi.org/10.1029/2003JE002182.

Racki, Grzegorz, et al. "Ernst Julius Öpik's (1916) Note on the Theory of Explosion Cratering on the Moon's Surface—The Complex Case of a Long-Overlooked Benchmark Paper." *Meteoritics & Planetary Science*, vol. 49, no. 10, 2014, pp. 1851–74. *Wiley Online Library*, https://doi.org/10.1111/maps.12367.

Robinson, M. S., J. W. Ashley, et al. "Confirmation of Sublunarean Voids and Thin Layering in Mare Deposits." *Planetary and Space Science*, vol. 69, no. 1, 1, Aug. 2012, pp. 18–27. *ScienceDirect*, https://doi.org/10.1016/j.pss.2012.05.008.

Robinson, M. S., S. M. Brylow, et al. "Lunar Reconnaissance Orbiter Camera (LROC) Instrument Overview." *Space Science Reviews*, vol. 150, no. 1, 1, Jan. 2010, pp. 81–124. *Springer Link*, https://doi.org/10.1007/s11214-010-9634-2.

Runyon, K. D., et al. "Impact Melt Facies in the Moon's Crisium Basin: Identifying, Characterizing, and Future Radiogenic Dating." *Journal of Geophysical*

Research: Planets, vol. 125, no. 1, 1, 2020, p. e2019JE006024. *Wiley Online Library*, https://doi.org/10.1029/2019JE006024.

Schnuriger, N., et al. "Long-Lived Volcanism Expressed through Mare Infilling, Domes and IMPs in the Arago Region of the Moon." *Planetary and Space Science*, vol. 185, June 2020, p. 104901. *ScienceDirect*, https://doi.org/10.1016/j.pss.2020.104901.

Singh, Tanu, and Neeraj Srivastava. "Geology of Grimaldi Basin on the Moon: Evidence for Volcanism and Tectonism during the Copernican Period." *Icarus*, vol. 351, Nov. 2020, p. 113921. *ScienceDirect*, https://doi.org/10.1016/j.icarus.2020.113921.

Small-Scale Lunar Graben: Distribution, Dimensions, and Formation Processes - ScienceDirect. https://www.sciencedirect.com/science/article/pii/S0019103514007222?via%3Dihub. Accessed 30 Dec. 2021.

Smith, David E., et al. "Initial Observations from the Lunar Orbiter Laser Altimeter (LOLA)." *Geophysical Research Letters*, vol. 37, no. 18, 18, 2010. *Wiley Online Library*, https://doi.org/10.1029/2010GL043751.

Solomon, Sean C., and James W. Head. "Vertical Movement in Mare Basins: Relation to Mare Emplacement, Basin Tectonics, and Lunar Thermal History." *Journal of Geophysical Research: Solid Earth*, vol. 84, no. B4, B4, 1979, pp. 1667–82. *Wiley Online Library*, https://doi.org/10.1029/JB084iB04p01667.

Stopar, Julie D., et al. “Occurrence and Mechanisms of Impact Melt Emplacement at Small Lunar Craters.” *Icarus*, vol. 243, Nov. 2014, pp. 337–57. *ScienceDirect*, https://doi.org/10.1016/j.icarus.2014.08.011.

Thesniya, P. M., and V. J. Rajesh. “Pyroxene Chemistry and Crystallization History of Basaltic Units in the Mare Humorum on the Nearside of the Moon: Implications for the Volcanic History of the Region.” *Planetary and Space Science*, vol. 193, Nov. 2020, p. 105093. *ScienceDirect*, https://doi.org/10.1016/j.pss.2020.105093.

Tognon, Gloria, et al. “Geologic Mapping and Age Determinations of Tsiolkovskiy Crater.” *Remote Sensing*, vol. 13, no. 18, 18, Jan. 2021, p. 3619. *www.mdpi.com*, https://doi.org/10.3390/rs13183619.

Watters, Thomas R., et al. “Shallow Seismic Activity and Young Thrust Faults on the Moon.” *Nature Geoscience*, vol. 12, no. 6, June 2019, pp. 411–17. *www.nature.com*, https://doi.org/10.1038/s41561-019-0362-2.

Williams, Kevin K., and Maria T. Zuber. “Measurement and Analysis of Lunar Basin Depths from Clementine Altimetry.” *Icarus*, vol. 131, no. 1, 1, Jan. 1998, pp. 107–22. *ScienceDirect*, https://doi.org/10.1006/icar.1997.5856.

Wilson, Lionel, and James W. Head. “Eruption of Magmatic Foams on the Moon: Formation in the Waning Stages of Dike Emplacement Events as an Explanation of ‘Irregular Mare Patches.’” *Journal of Volcanology and Geothermal Research*, vol. 335, Apr. 2017, pp. 113–27. *ScienceDirect*, https://doi.org/10.1016/j.jvolgeores.2017.02.009.

Wood, Charles A. “Scientific Knowledge of the Moon, 1609 to 1969.” *Geosciences*, vol. 9, no. 1, 1, 2019, p. 5. *ProQuest*, http://dx.doi.org/10.3390/geosciences9010005.

Wu, Yun-Zhao, et al. “Space Weathering of the Moon from in Situ Detection.” *Research in Astronomy and Astrophysics*, vol. 19, no. 4, Apr. 2019, p. 051. *Institute of Physics*, https://doi.org/10.1088/1674-4527/19/4/51.

Wünnemann, K., et al. “Numerical Modelling of Impact Melt Production in Porous Rocks.” *Earth and Planetary Science Letters*, vol. 269, no. 3, 3, May 2008, pp. 530–39. *ScienceDirect*, https://doi.org/10.1016/j.epsl.2008.03.007.

Xiao, Zhiyong, et al. “Cooling Fractures in Impact Melt Deposits on the Moon and Mercury: Implications for Cooling Solely by Thermal Radiation.” *Journal of Geophysical Research: Planets*, vol. 119, no. 7, 7, 2014, pp. 1496–515. *Wiley Online Library*, https://doi.org/10.1002/2013JE004560.

Yan, Bokun, et al. “Mapping Lunar Global Chemical Composition from Chang’E-1 IIM Data.” *Planetary and Space Science*, vol. 67, no. 1, July 2012, pp. 119–29. *ScienceDirect*, https://doi.org/10.1016/j.pss.2012.03.010.

Zanetti, M., et al. *Aristarchus Crater: Mapping of Impact Melt and Absolute Age Determination*. 2011.